

Galactic Model Parameters and Space Density of Cataclysmic Variables in Gaia Era: New Constraints to Population Models

REMZIYE CANBAY,¹ SELÇUK BILIR,² AYKUT ÖZDÖNMEZ,³ AND TANSEL AK²

¹*Istanbul University, Institute of Graduate Studies in Science, Programme of Astronomy and Space Sciences, 34116, Beyazıt, Istanbul, Turkey*

²*Istanbul University, Faculty of Science, Department of Astronomy and Space Sciences, 34119, Beyazıt, Istanbul, Turkey*

³*Atatürk University, Faculty of Science, Department of Astronomy and Space Sciences, 25240, Erzurum, Turkey*

(Received January 05, 2023; Revised February 16, 2023; Accepted February 21, 2023)

Submitted to AJ

ABSTRACT

The spatial distribution, Galactic model parameters and luminosity function of cataclysmic variables (CVs) are established using re-estimated trigonometric parallaxes of *Gaia* DR3. The data sample of 1,587 CVs in this study is claimed to be suitable for Galactic model parameter estimation as the distances are based on trigonometric parallaxes and the *Gaia* DR3 photometric completeness limits were taken into account when the sample was created. According to the analysis, the scale height of All CVs increases from 248 ± 2 to 430 ± 4 pc towards shorter periods near the lower limit of the period gap and suddenly drops to 300 ± 2 pc for the shortest orbital period CVs. The exponential scale heights of All CVs and magnetic systems are found to be 375 ± 2 and 281 ± 3 pc, respectively, considerably larger than those suggested in previous observational studies. The local space density of All CVs and magnetic systems in the sample are $6.8_{-1.1}^{+1.3} \times 10^{-6}$ and $2.1_{-0.4}^{+0.5} \times 10^{-6}$ pc⁻³, respectively. Our measurements strengthen the 1-2 order of magnitude discrepancy between CV space densities predicted by population synthesis models and observations. It is likely that this discrepancy is due to objects undetected by CV surveys, such as the systems with very low \dot{M} and the ones in the period gap. The comparisons of the luminosity function of white dwarfs with the luminosity function of All CVs in this study show that 500 times the luminosity function of CVs fits very well to the luminosity function of white dwarfs. We conclude that the estimations and data sample in this study can be confidently used in further analysis of CVs.

Keywords: Cataclysmic Variables – solar neighbourhood

1. INTRODUCTION

Cataclysmic variables (CVs) are short-period semi-detached binary stars. A cataclysmic variable's primary component is a white dwarf which is accreting matter from a Roche-lobe filling low-mass main-sequence star, the secondary component, via a gas stream. Since the matter stream has a high angular momentum and the primary star is small, an accretion disc surrounding the white dwarf is created. A bright spot is also formed where the matter stream impacts the disc. Magnetised white dwarfs in CVs have accretion columns instead of discs to transfer matter from the secondary component (Warner 1995; Hellier 2001; Knigge 2011; Knigge, Baraffe & Patterson 2011).

The standard formation and evolution scenario developed for CVs is concentrated on the explanation of the features seen in the orbital period distribution of these systems, since the most precisely determined parameter of a CV is its orbital period. The sharp cut-off at about 80 min (Willems et al. 2005; Gänsicke et al. 2009), period minimum, and the period gap between roughly 2 and 3 h (King 1988; Knigge, Baraffe & Patterson 2011) are the most striking features

of the CV period distribution. The standard theory successfully explains these features as its main predictions are supported by observations. However, there are still some observational properties to be explained, for example (1) Predicted and observed fractions of CVs above and below the period gap (de Kool 1992; Kolb 1993; Howell, Nelson & Rappaport 2001; Gänsicke et al. 2009; McAllister et al. 2019) are not in agreement. Standard CV population studies predict that more than 90% of CVs must be located below the period gap, while observations imply almost equal numbers of CVs below and above the gap. Although sky surveys like the Sloan Digital Sky Survey (SDSS; Szkody et al. 2002, 2003, 2004, 2005, 2006, 2007, 2011) revealed a larger population of short-period CVs, the disagreement still remains. (2) The fraction of observed post-period minimum CVs, period bouncers, is much smaller than that predicted by the population models based on the standard theory (Patterson et al. 2005; Unda-Sanzana et al. 2008; Littlefair et al. 2008; Patterson 2011; Kato et al. 2015, 2016; McAllister et al. 2017; Neustroev et al. 2017; Pala et al. 2018). McAllister et al. (2019) found that 30% of donor stars in a sample of 225 CVs are likely to be brown dwarfs in period bouncers. However, only 5% of volume-limited sample of CVs in Pala et al. (2020) included period bouncers. (3) Although the standard theory predicts an orbital period minimum of about 65-70 min (see Kalomeni et al. 2016, and references therein), observed values are about 76-82 min (Knigge, Baraffe & Patterson 2011; McAllister et al. 2019). (4) The observed white dwarf masses in CVs have been significantly larger than those of single white dwarfs (see Zorotovic & Schreiber 2020, and references therein). In addition, white dwarf mass in CVs does not change with orbital period (McAllister et al. 2019). (5) Population studies based on the standard evolutionary model predict space densities 1-2 orders of magnitude larger than observed values (Zorotovic & Schreiber 2020). Although additional angular momentum loss mechanisms and models (Patterson 1998; Knigge, Baraffe & Patterson 2011; Schreiber, Zorotovic & Wijnen 2016; Pala et al. 2017; Zorotovic & Schreiber 2017, 2020; Belloni et al. 2018; Liu & Li 2019; Metzger et al. 2021; Sarkar & Tout 2022) were suggested to solve the disagreements, the only published, self-consistent simulations of CV evolution were performed by Hillman et al. (2020), whose multi-Gyr models of novae take into account every nova eruption's thermonuclear runaway, mass and angular momentum losses, feedback due to irradiation and variable mass transfer rate (\dot{M}), and orbital size and period changes. Hillman et al. (2020) reproduced the observed range of mass transfer rates at a given orbital period, with large and cyclic Kyr-Myr timescale changes. It should be noted that the magnetic systems may have different evolutionary scenarios from non-magnetic CVs (see references in Belloni et al. 2020).

Depending on the completeness of the samples, reliable observational constraints can be obtained from the stellar statistics (Ak et al. 2008; Özdönmez, Ak & Bilir 2015), and a proposed evolutionary scheme must also be in agreement with the data obtained from stellar statistics (Duerbeck 1984). In this respect, Galactic model parameters and the space density of a group of objects are key parameters to constrain and to test population models based on evolutionary schemes. A wide range of observational results is remarkable, while the predicted space densities are systematically 1-2 order of magnitude larger than those derived from observations. For example, previous CV population synthesis models predicted space densities 10^{-5} - 10^{-4} pc $^{-3}$ (Ritter & Burkert 1986; de Kool 1992; Kolb 1993; Politano 1996; Willems et al. 2005, 2007; Goliaş & Nelson 2015; Belloni et al. 2018), while observations indicated 10^{-7} - 10^{-4} pc $^{-3}$ (Warner 1974; Patterson 1984, 1998; Thomas & Beuermann 1998; Ringwald 1993; Schwöpe et al. 2002; Araujo-Betancor et al. 2005; Pretorius et al. 2007a; Pretorius, Knigge & Kolb 2007b; Ak et al. 2008; Revnivtsev et al. 2008; Pretorius & Knigge 2012; Pretorius, Knigge & Schwöpe 2013; Schwöpe 2018). In a recent study, Pala et al. (2020) measured very precise space densities of $4.8_{-0.9}^{+0.6} \times 10^{-6}$ and $1.2_{-0.5}^{+0.4} \times 10^{-6}$ pc $^{-3}$ for All CVs and magnetic CVs (mCVs), respectively, using the European Space Agency's (ESA) *Gaia* Data Release 2 (*Gaia* DR2; *Gaia* Collaboration 2018). They assumed a scale height of 280 pc for their analysis and the sample was composed of only 42 objects within 150 pc from the Sun. They assumed that this restriction reduces the uncertainties in the derived space densities related to the unknown age and scale height of the CV population and the uncertainties from astrometric solutions. Belloni et al. (2020) claimed that these are the most reliable observational space density estimates ever found. They also concluded that the space densities given in Pala et al. (2020) are in very good agreement with their predicted values if potential period bouncers are excluded from the space density estimation. However, it should be noted that Belloni & Schreiber (2020) performed binary population models using an up-to-date version of the BSE code (Hurley, Tout & Pols 2002) and found that their model fails to explain some observational properties of magnetic CVs. Thus, the agreement between the space density measurements of Pala et al. (2020) and predictions by Belloni et al. (2020) does not mean that the previous population synthesis models based on the standard evolution and formation theory are wrong. It is likely that the space densities of 10^{-5} - 10^{-4} pc $^{-3}$ proposed by previous CV population synthesis models are correct and the current observational measurements suffer from incomplete sky surveys as the surveys are probably missing the most of very

low \dot{M} systems, CVs in the orbital period gap, whose lifetime is predicted to be longer (Hillman et al. 2020), and the most of period bouncers.

Besides these studies, observational Galactic model parameters, luminosity functions and space densities of CVs, i.e. intrinsic properties of Galactic CV population, should still be determined from suitable data by using the methods of observational Galactic structure studies (Karaali, Bilir & Hamzaoglu 2004; Bilir et al. 2006a,b; Bilir, Karaali & Gilmore 2006c; Bilir et al. 2008; Karaali et al. 2007; Cabrera-Lavers et al. 2007), as the number of systems with reliable distance estimates is high enough to use these methods. Sky surveys such as *Gaia* (Gaia Collaboration 2016, 2018, 2021a, 2022) and SDSS (Szkody et al. 2002, 2003, 2004, 2005, 2006, 2007, 2011) determined faint systems and presented reliable distances of CVs. Using these data, it is possible to decrease the selection effects that may be strong for faint systems. These data and methods can allow us to determine observational constraints for evolutionary models of CVs and mCVs.

In this study, we use ESA’s *Gaia* Data Release 3 (*Gaia* DR3; Gaia Collaboration 2022) and Bailer-Jones et al. (2021) to obtain reliable distances for a CV sample. We analyse the spatial distribution of CVs and discuss the completeness of the CV sample. Then, we use this sample to estimate the Galactic model parameters and space densities of All CVs and mCVs with scale-heights obtained from exponential and sech^2 functions fitted to z -histograms.

2. DATA

In order to construct our CV sample, we collected CVs from AAVSO’s International Variable Star Index¹ database. Their equatorial and Galactic coordinates were taken from SIMBAD² database. We also included CV’s found in the previous studies (e.g. Hofmann et al. 2018; Halpern et al. 2018; Szkody et al. 2018; Bernardini et al. 2019; Kato 2019; Yu et al. 2019; Belloni et al. 2020; Kato et al. 2020; Schwöpe et al. 2020) in this sample. Orbital periods were mainly taken from Ritter & Kolb (2003) and Downes et al. (2001). Superhump periods of objects, whose orbital periods are unknown, were assumed to be their orbital periods (Kato et al. 2020, and references therein). The number of systems is 10,852 in this very rough sample. We ignored the objects classified as non-mCVs and removed objects for which trigonometric parallax measurements are not present in *Gaia* DR3. All the objects in the preliminary sample were checked with respect to equatorial coordinates in order to avoid from duplication. In order to prevent the misidentification of CVs due to adjacent objects, we also checked each object’s *Gaia* position individually using Aladin³ and removed misidentified objects from the database. To ensure a robust match, we crossmatched each object in the catalogue to a 15'' radius in *Gaia* DR3, propagated the subsets of *Gaia* DR3 15'' crossmatches to the J2000 epoch using proper motion, and made a final crossmatch at J2000 with a radius of 2'', given the precision of the catalogue. The 132 CVs in the directions of the globular clusters were excluded from the statistics to avoid mismatching with the data in the *Gaia* catalogue. As a result of this selection process, *Gaia* photometric and astrometric data of 5,621 CVs were obtained. We showed the matching procedure for nine objects as an example. The results for matching these objects at different G apparent magnitudes from the *Gaia* DR3 catalogue with panSTARR g images on Aladin⁴ are shown in Figure 1.

As we need a precise data sample to extract Galactic model parameters of CVs, we also made strict cuts on quality flags, even though these cuts remove numerous systems from the sample. We retain matches with `phot_g_mean_flux_over_error`, $f_G/\delta f_G > 8$, more than eight “good” astrometric observations, as characterized by *Gaia* DR3, `astrometric_excess_noise` < 2, and $\varpi > 0.1$ mas. The remaining sample includes 4,149 CVs. In the sample, magnetic CVs classified as DQ Her (Intermediate polars) or AM Her type (Polars) objects are indicated as mCV, remaining systems as CV. Number of magnetic CVs is only 205 in this sample. Although the sample includes 4,149 objects classified as CV, we know orbital periods only for 1,187 of them.

We used *Gaia* DR3 data (Gaia Collaboration 2022) to obtain the distances of CVs in our catalogue. In order to do this, we matched our catalogue with *Gaia* DR3 catalogue and found *Gaia* ID for each CV. It is possible to estimate the distances of CVs by simply inverting their trigonometric parallaxes taken from *Gaia* DR3 catalogue. However, Bailer-Jones et al. (2018, 2021) indicated that the nonlinearity of the transformation and the asymmetry of the resulting probability distribution must be taken into account, and they re-estimated the *Gaia* EDR3 (Gaia Collaboration 2021a) parallaxes. In such a re-estimation, we do not expect too different distance estimates from *Gaia* DR3 data and Bailer-Jones et al. (2021)’s approximation for a certain system. Thus, we matched our catalogue with

¹ www.aavso.org/vsx/

² <https://simbad.u-strasbg.fr/simbad/sim-fid>

³ <https://aladin.u-strasbg.fr/AladinLite/>

⁴ <http://aladin.cds.unistra.fr/aladin.gml>

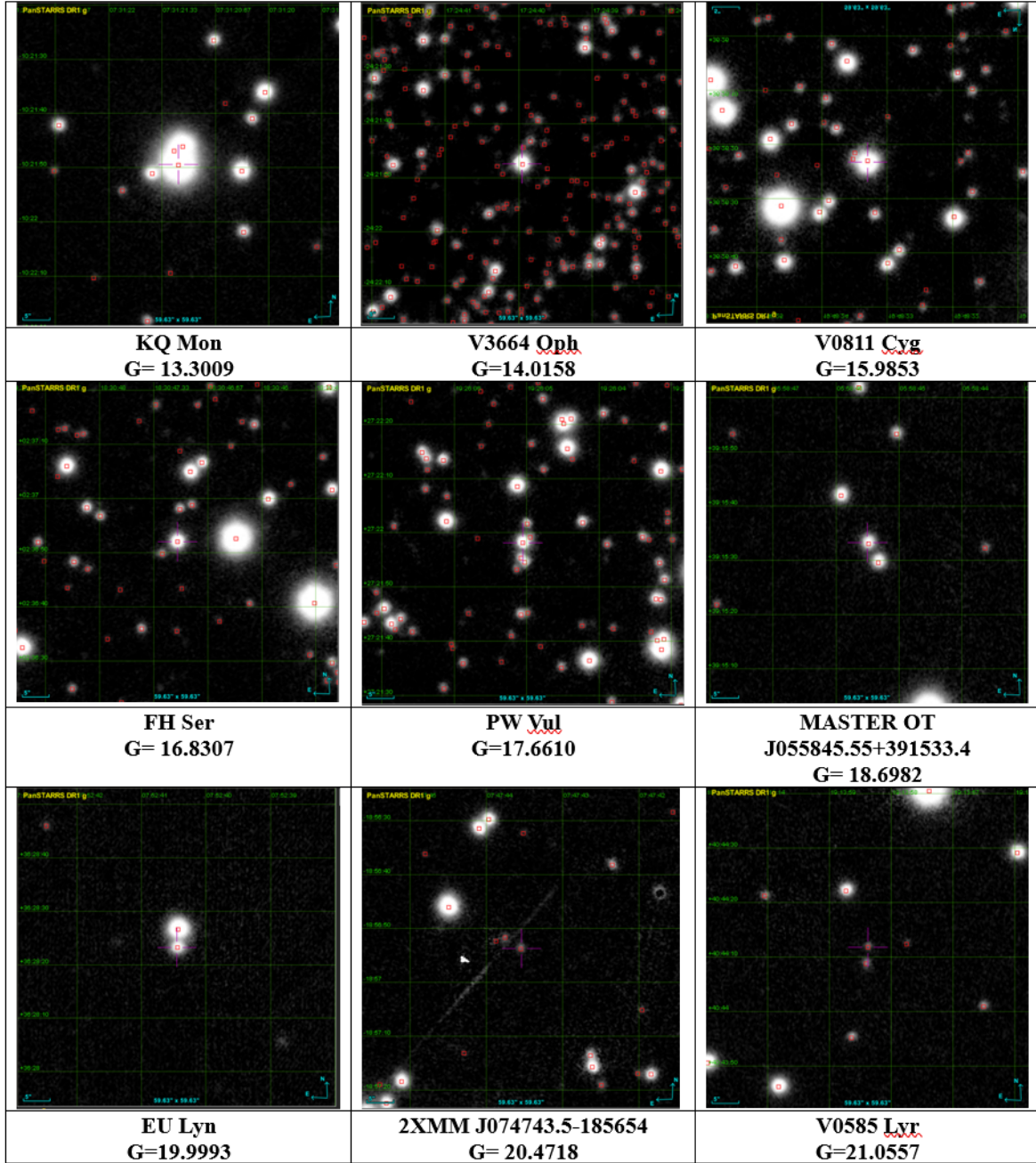


Figure 1. Location of nine CVs with different G apparent magnitudes selected from the *Gaia* DR3 catalogue are shown on panSTARR g images using Aladin. Target objects are located in the centres of the images.

the catalogue of Bailer-Jones et al. (2021) using *Gaia* DR3 IDs to obtain precise distances and distance errors of CVs and compared distances of CVs estimated from *Gaia* DR3 and Bailer-Jones et al. (2021) in Figure 2, where different G apparent magnitude intervals are represented by coloured symbols. This comparison shows that there is a considerable scatter especially for fainter systems, while the scatter is much less for CVs with $G \leq 18.5$ mag. Thus, we limited our CV sample to the systems for which $G \leq 18.5$ mag, which is set as the faint limit of the sample. We set the bright limit as $G = 9$ mag, since there is no brighter object in our sample. The final sample comprises of CVs with $9 \leq G \leq 18.5$ mag and includes 1,714 CVs, 767 of them with known orbital periods. The relative distance error of the sample is less than 1.66 and the median value is 0.06.

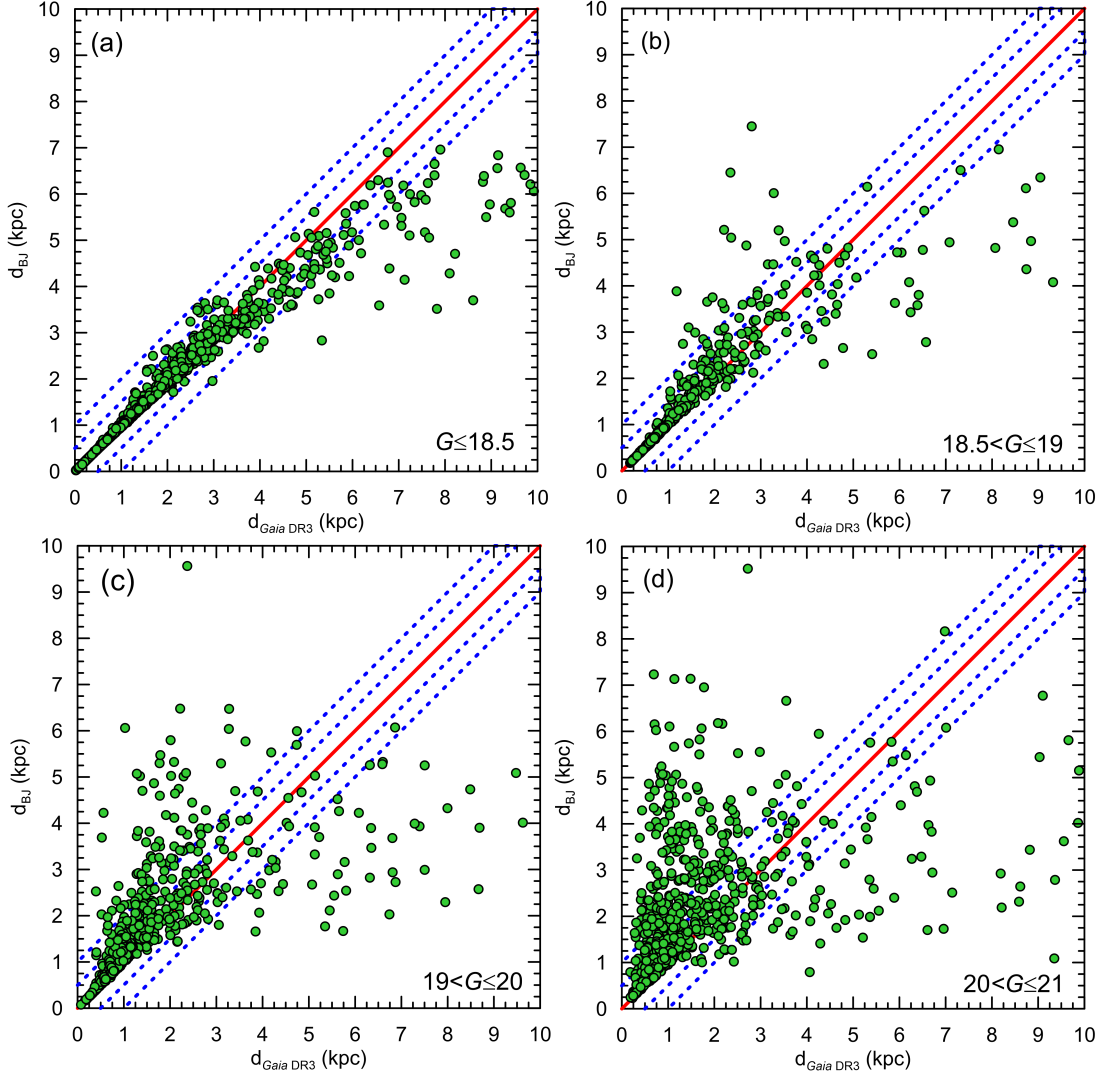


Figure 2. Comparison of CV distances obtained from *Gaia* DR3 and Bailer-Jones et al. (2021) (d_{BJ}). Different G apparent magnitude intervals are shown in panels (a), (b), (c) and (d). The red line represents the one-to-one line and blue dashed lines 500 and 1000 pc distances from the red line.

Although the number of CVs in the sample is the largest ever used in similar analyses, it is still questionable if this sample is sufficiently large to be representative of the entire CV population and subject to magnitude-related selection effects. Since the standard theory predicts that most CVs should be intrinsically faint objects, it seems that apparent magnitude limits of surveys are one of the strongest selection effects. Therefore, the completeness limits of the data must be taken into account in a study based on stellar statistics.

In order to set completeness limits to the sample, we first obtained interstellar absorption in V -band A_V for CVs in the sample by using MWDUST⁵ code which produces two and three-dimensional Galactic dust map (Bovy et al. 2016), based on Schlegel, Finkbeiner & Davis (1998)’s dust maps as re-calibrated by Schlafly & Finkbeiner (2011). MWDUST code can provide two and three-dimensional data according to Galactic coordinates from the Sun to all directions until the edges of our Galaxy contributed by the Galactic dust. Since the distances of systems are well-known from trigonometric parallaxes, we preferred to use two-dimensional data and showed the rough absorption value in V -band according to Galactic latitude (b) and longitude (l) toward the direction of an object by $A_\infty(V)$, practically means up to infinite, but actually up to the edge of the Galaxy.

⁵ <https://github.com/jobovy/mwdust>

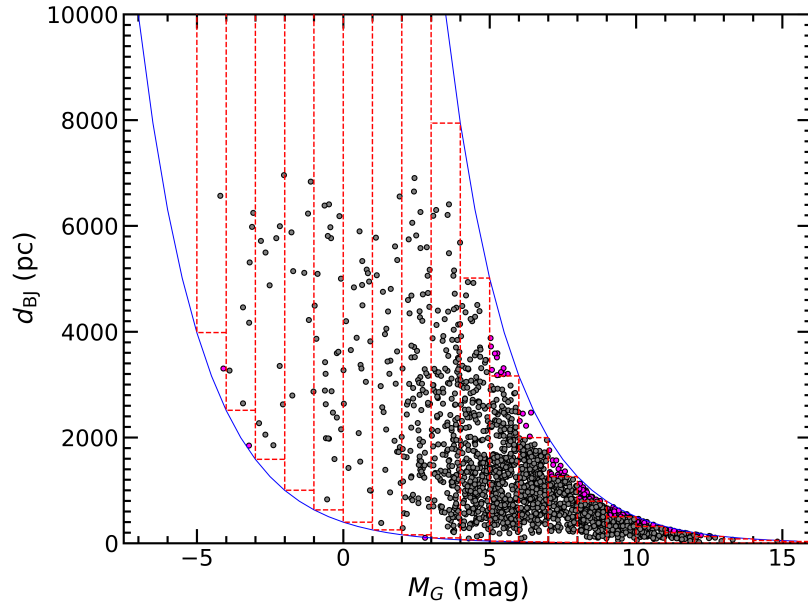


Figure 3. The absolute magnitudes M_G of CVs in the preliminary sample against their distances d_{BJ} obtained from [Bailer-Jones et al. \(2021\)](#). Red dashed lines show distances estimated from the bright ($G = 9$ mag) and faint ($G = 18.5$ mag) limiting apparent magnitudes for absolute magnitude intervals of 1 mag. Blue solid lines correspond to the bright and faint apparent magnitude limits.

The total absorption in V -band for the distance d to the star is calculated as following ([Bahcall and Soneira 1980](#))

$$A_d(V) = A_\infty(V) \left[1 - \exp\left(\frac{-|d \times \sin b|}{H}\right) \right], \quad (1)$$

here H is the scaleheight for the interstellar dust which is adopted as 125 pc ([Marshall et al. 2006](#)). As the distance of the system (d_{BJ} , hereafter also denoted as d) d is known from [Bailer-Jones et al. \(2021\)](#), the total absorption for the system $A_d(V)$ could be estimated. We obtained the colour excess $E_d(B - V)$ for each CV in the sample using $E_d(B - V) = A_d(V)/3.1$. The total absorptions in G , G_{BP} , and G_{RP} bands were obtained by using relations given as follows:

$$\begin{aligned} A(G) &= 0.83627 \times 3.1 E_d(B - V), \\ A(G_{\text{BP}}) &= 1.08337 \times 3.1 E_d(B - V), \\ A(G_{\text{RP}}) &= 0.63439 \times 3.1 E_d(B - V). \end{aligned} \quad (2)$$

The selective absorption coefficients in Equation (2) were taken from [Cardelli, Clayton, & Mathis \(1989\)](#). Once we know the total absorption values, we could calculate the de-reddened apparent magnitudes in G , BP and RP -bands, G_0 , G_{BP} and G_{RP} , respectively. The absolute magnitudes M_G of CVs were calculated using the distance modulus formula $G_0 - M_G = 5 \times \log(d_{\text{BJ}}) - 5$, where d_{BJ} is the distance obtained from [Bailer-Jones et al. \(2021\)](#). The absolute magnitudes M_G of CVs in the preliminary sample against their distances are shown in Figure 3.

Red dashed lines in Figure 3 show distances estimated from the bright and faint brightness limits ($9 \leq G \leq 18.5$ mag) for absolute magnitude intervals of 1 mag. These boxes limited by red dashed lines define the completeness limits of the data for certain absolute magnitude intervals. We removed systems beyond (out of the boxes defined by red dashed lines in Figure 3) these limiting magnitudes from the CV sample in order to obtain a complete catalogue in a certain volume with the Sun in its centre. We found that the majority of systems beyond 4 kpc in Figure 3 are discovered by SDSS. The final sample includes 1,587 CVs, 704 of them with known orbital periods. There are only 124 mCVs in this sample, 117 of them with a known orbital period. Analyses in this paper were performed using this final sample.

Table 1. The data sample. The object name, equatorial coordinates $(\alpha, \delta)_{J2000}$, orbital periods P_{orb} and object groups (magnetic (mCV) or non-magnetic (non-mCVs)). G denotes G -band apparent magnitudes, $\bar{\omega}$ trigonometric parallaxes, $\sigma_{\bar{\omega}}/\bar{\omega}$ relative parallax errors, $\mu_{\alpha} \cos \delta$ and μ_{δ} proper motion components from *Gaia* DR3. Distance d_{BJ} is calculated using the system parallax in Bailer-Jones et al. (2021). First and the last two rows of Table 1 is given here. The table can be obtained electronically.

ID	Star Name	α	δ	Object groups	P_{orb} (d)	$\bar{\omega}$ (mas)	$\sigma_{\bar{\omega}}/\bar{\omega}$	$\mu_{\alpha} \cos \delta$	μ_{δ}	G (mag)	d_{BJ} (pc)	Ref
		(hh:mm:ss)	(dd:mm:ss)					(mas yr ⁻¹)	(mas yr ⁻¹)			
0001	2XMM J000134.1+625008	00 01 34.18	+62 50 07.40	non-mCVs	0.2519	0.0968	2.268±0.091	0.486±0.0941	17.9224±0.0043	4133±1764
0002	EF Tuc	00 01 55.10	-67 07 43.3	non-mCVs	0.145	0.7120	0.0203	13.348±0.020	-1.455±0.0230	14.8480±0.0196	1330±36	(01)
....
....
....
....
1713	2dFGRS TGS429Z114	23 50 32.90	-31 25 48.5	non-mCVs	-	0.2672	0.0585	-2.237±0.043	-3.851±0.045	16.6399±0.0028	3338±715
1714	BC Cas	23 51 17.45	+60 18 10.0	non-mCVs	-	0.5360	0.0588	-0.861±0.059	-2.52±0.06	17.2256±0.0095	1831±198

(01) Downes et al. (2001), (02) Hardy et al. (2017), (03) Ritter & Kolb (2003), (04) Szkody et al. (2013), (05) González-Buitrago et al. (2013), (06) Steiner et al. (2007), (07) Paterson et al. (2019), (08) Kozhevnikov (2019), (09) Thorstensen et al. (2017), (10) Watson, Henden, & Price (2006), (11) Wils et al. (2011), (12) Thorstensen, Alper, & Weil (2016), (13) Rude & Ringwald (2012), (14) Nesci, Tuvikene, & Gualandi (2019), (15) Patterson et al. (2003), (16) Hamilton-Drager et al. (2018), (17) Sterken et al. (2007), (18) Thorstensen (2020), (19) Coppejans et al. (2016), (20) Plavchan et al. (2008), (21) Copperwheat et al. (2011), (22) Shafter & Misselt (2006), (23) Bruch (2019), (24) Masci et al. (2019), (25) Hümmelich, Bernhard, & Srdoc (2014), (26) McAllister et al. (2015), (27) Thorstensen et al. (2020), (28) Kato et al. (2015), (29) Kozhevnikov (2014), (30) Thorstensen & Fenton (2003), (31) Drake et al. (2014), (32) Thorstensen, Peters, & Skinner (2010), (33) Schaefer (2021), (34) Ruiz-Carmona, Groot, & Steeghs (2020), (35) Kato et al. (2009), (36) Kozhevnikov (2018), (37) Pala et al. (2020), (38) Halpern & Thorstensen (2015), (39) Alfonso-Garzón et al. (2012), (40) Rodríguez-Gil et al. (2012), (41) Kato et al. (2017), (42) Kozhevnikov (2003), (43) Halpern et al. (2018), (44) Worpel et al. (2018), (45) Kato (2020), (46) Rodríguez-Gil & Torres (2005), (47) Thorstensen & Skinner (2012), (48) Joshi et al. (2020), (49) Dai et al. (2020), (50) Bernardini et al. (2019), (51) Bruch & Diaz (2017), (52) Belloni et al. (2020), (53) McAllister et al. (2019), (54) Mason et al. (2013), (55) Uemura et al. (2010), (56) Beuermann et al. (2021), (57) Samus' et al. (2017), (58) Kato et al. (2020), (59) Pal et al. (2020), (60) Tappert et al. (2013), (61) Vogt et al. (2018), (62) Rutkowski et al. (2011), (63) Avilés et al. (2020), (64) Chen et al. (2020), (65) Koen & O'Donoghue (1995), (66) Gabdeev et al. (2019), (67) Ringwald & Velasco (2012), (68) Han et al. (2016), (69) Mukai, Zietsman, & Still (2009), (70) Hamsch (2014), (71) Kato et al. (2013), (72) Bond & Miszalski (2018), (73) Zubareva et al. (2011), (74) Yu et al. (2019), (75) Sheets et al. (2007), (76) Breus, Petrik, & Zola (2019), (77) Gasque et al. (2019), (78) Myers et al. (2017), (79) Kozhevnikov (2017), (80) Rude & Ringwald (2012a), (81) Altan et al. (2019), (82) Weil, Thorstensen, & Haberl (2018)

The final sample is given in Table 1 including equatorial coordinates $(\alpha, \delta)_{J2000}$, object groups (magnetic (mCVs) or non-magnetic (non-mCVs)), orbital periods (P_{orb}), *Gaia* DR3 trigonometric parallaxes ($\bar{\omega}$) and relative parallax errors ($\sigma_{\bar{\omega}}/\bar{\omega}$), proper motions ($\mu_{\alpha} \cos \delta$, μ_{δ}), G -band apparent magnitudes from *Gaia* DR3. Distances d_{BJ} (also denoted as d) in Table 1 were taken from Bailer-Jones et al. (2021). This sample is the largest ever used in similar analyses of CVs. Besides, it includes the most reliable distance information for these systems. Objects, that are not classified as magnetic system in the literature, are denoted as CV in our catalogue.

In Figure 4a, we show the distance histogram of CVs in the final sample which is limited using bright and faint limiting magnitudes in G -band, 9 and 18.5 mag, respectively. The cumulative distribution of CV distances is presented in Figure 4b. Relative distance errors $\sigma_{d_{\text{BJ}}}/d_{\text{BJ}}$ obtained from Bailer-Jones et al. (2021) are also shown in Figure 4c. As expected, the relative errors are increasing with the distance. Relative distance errors are good indicators of the precision of the distance measurements, which is very important in our study. While relative errors for 66% of the systems in the final sample is $\sigma_{d_{\text{BJ}}}/d_{\text{BJ}} \leq 0.10$, 88% of them have relative distance errors of $\sigma_{d_{\text{BJ}}}/d_{\text{BJ}} \leq 0.25$. These values show that reliable constraints to population models of CVs can be obtained from the sample in this study.

Precision of distance estimations can be also seen in the HR diagram of CVs, for which the orbital periods are known. Figure 5 shows HR diagram of CVs below and above the orbital period gap using *Gaia* photometry. The separating point of the orbital period gap is accepted as 2.6 h (Ak et al. 2010). CVs above the gap are generally brighter than those located below, as expected. This discrimination is very clear now due to precise distance measurements. It is clear that colour range for systems with $P_{\text{orb}} \leq 2.6$ h is narrower compared to that of systems with $P_{\text{orb}} > 2.6$ h. Figure 5 shows that there are short-period systems brighter than $M_G \approx 5$ mag. These are probably SU UMa type dwarf novae, which were in the superoutburst phase when they were observed. Blue and grey shaded parts in the HR diagram of CVs represent the regions where the white dwarf, main sequence and giant stars are located, respectively. The data for these shaded regions were taken from Abril et al. (2020).

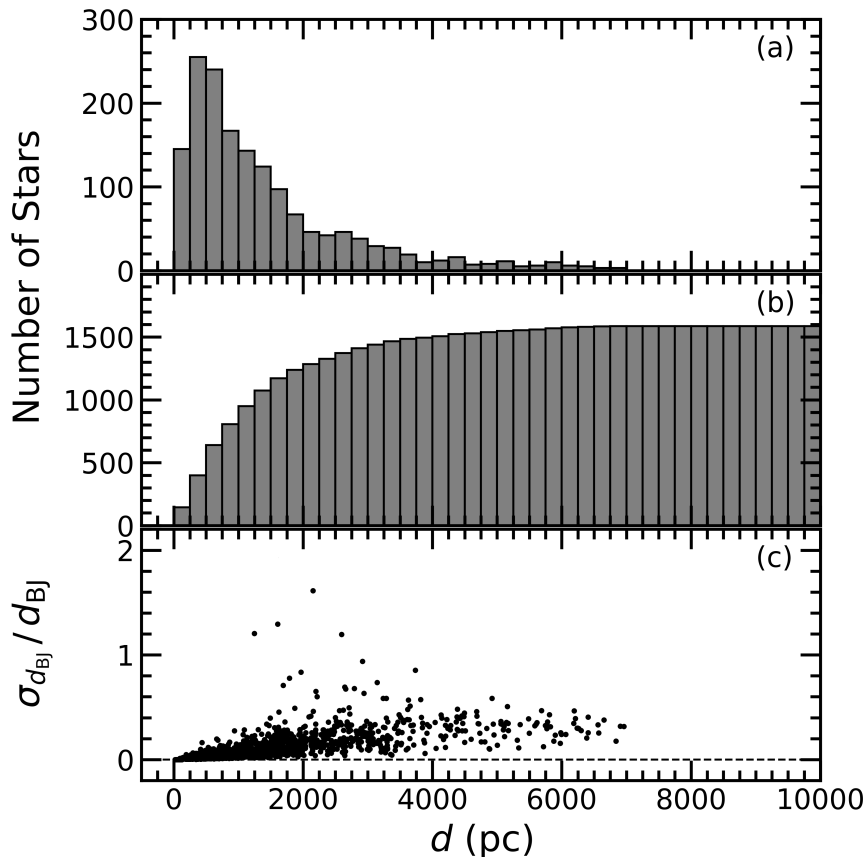


Figure 4. Distance histogram of CVs in the sample which is limited using bright and faint limiting magnitudes in G -band. Relative distance errors $\sigma_{d_{\text{BJ}}}/d_{\text{BJ}}$ are also shown in the lowest panel.

Table 2. The median distances (d) and heliocentric rectangular Galactic coordinates (X , Y , Z) of CVs in the sample. Values are separately listed for All CVs and magnetic (mCVs) systems. N denotes the number of objects.

Group	N	\tilde{d}	\tilde{X}	\tilde{Y}	\tilde{Z}
		(pc)	(pc)	(pc)	(pc)
All CVs	1587	989	80	93	-18
mCVs	124	559	-51	-4	24

3. THE ANALYSIS AND COMPARISONS

3.1. Spatial distribution

The distribution of CVs in the final sample according to equatorial and Galactic coordinates are plotted in Figure 6, upper and lower panels, respectively. The panels in Figure 6 indicate that the CVs are symmetrically distributed about the Galactic plane in general. The densest regions in both panels correspond to the Solar vicinity. In order to inspect the Galactic distribution of CVs in the Solar neighbourhood, we also calculated the Sun-centred rectangular Galactic coordinates of CVs (X towards Galactic centre, Y Galactic rotation, Z north Galactic pole) in the sample and displayed their projected positions on the Galactic plane ($X - Y$ plane) and on a plane perpendicular to it ($X - Z$ plane) in Figure 7. Median heliocentric rectangular Galactic coordinates (X , Y , Z) are 80, 93 and -18 pc, respectively, for all systems in the sample and -51, -4 and 24 pc for magnetic systems, respectively. These values are summarized in Table 2.

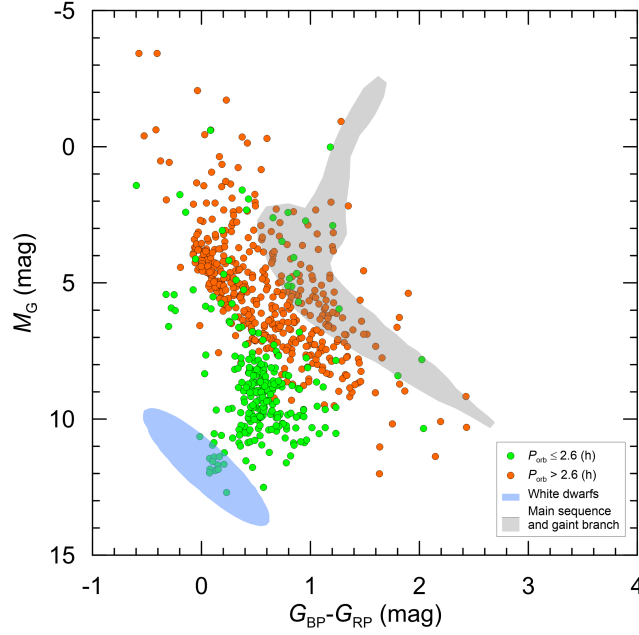


Figure 5. *Gaia* DR3 HR diagram of CVs for which orbital periods P_{orb} are known in the final sample. The separating point of the orbital period gap is accepted as 2.6 h (Ak et al. 2010). White dwarf, main-sequence and giant star regions are shaded in blue and grey, respectively (Abril et al. 2020).

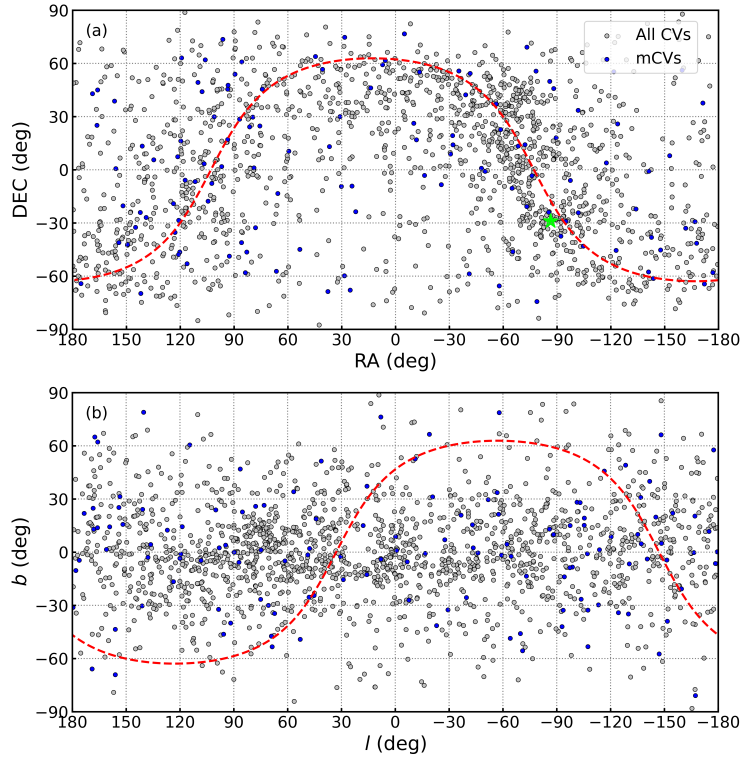


Figure 6. The distribution of CVs according to an equatorial (α , δ) and Galactic (l , b) coordinates. Distributions of magnetic and non-magnetic systems are shown with different colours, blue and black, respectively. Red dashed lines represent the Galactic plane (upper panel) and the celestial equator (lower panel). The green star in the upper panel indicates the location of the Galactic centre on the plot.

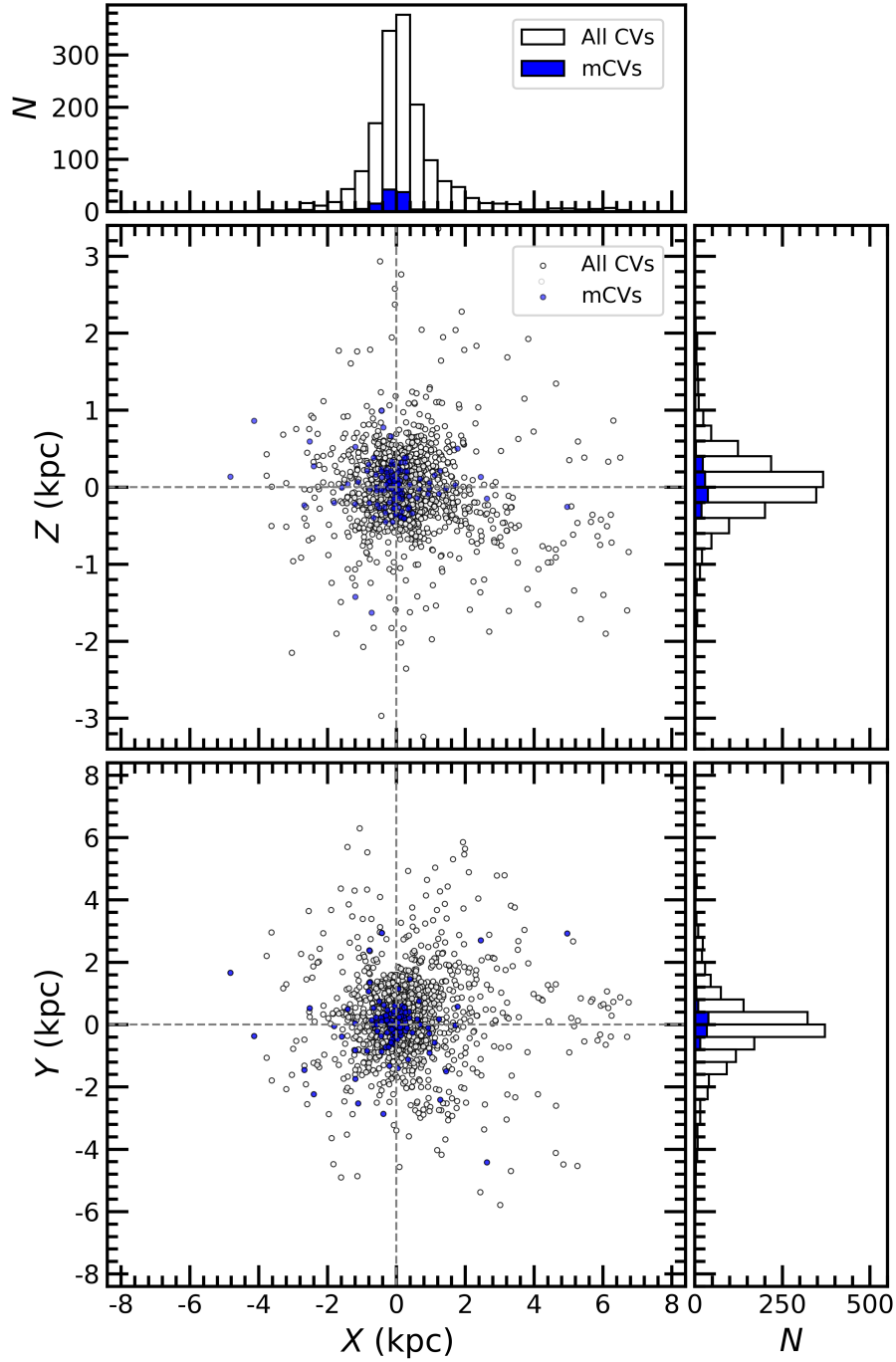


Figure 7. The spatial distribution of CVs in the final sample with respect to the Sun. X , Y and Z are the Sun centred rectangular Galactic coordinates. Magnetic systems (mCVs) are shown with blue symbols. Number histograms created according to coordinates are shown to the right and top of the figure.

Figures 6 and 7 show that there is no considerable bias according to the spatial distribution of CVs in our study. It should be noted that only magnetic CVs near the Sun can be detected as they are faint objects, in general. The median distances of CVs in the final sample are 989 and 559 pc for All CVs and magnetic systems, respectively. The median distances of All CVs and magnetic systems in the CV sample of [Özdönmez et al. \(2015\)](#) were found to be 423 and 385 pc, respectively. Comparisons of median distances in both studies and Figure 5 in this study with Figure 6

of Özdönmez et al. (2015) reveals that much farther objects are included in our sample, thanks to *Gaia* mission. In addition, the number of CVs with distance estimates in this study is higher, and the distances are more accurate than those in Özdönmez et al. (2015).

3.2. Galactic model parameters

Using the number of objects per unit volume, it is possible to obtain information on their Galactic population. Galactic locations of objects must be known in order to estimate their Galactic model parameters. This information allows us to estimate scale length and scale height of the objects in question. Based on deep sky surveys, it is known that the scale length of the thin disc stars is expected to be larger than 2.6 kpc (Bilir et al. 2006a; Juric et al. 2008). Besides All CVs being members of the thin-disc population of the Galaxy according to their Galactic kinematics (Ak et al. 2015), most of the systems in our sample are located in distances less than 2 kpc, as shown in Figure 7, and the median distance of All CVs in the final sample is 989 pc, which is much less than 2.6 kpc. Thus, our sample was not inspected according to population types and the scale length estimation was not performed.

In order to find the Galactic model parameters of CVs, z -histograms that demonstrate the vertical distribution of objects in the Galaxy must be studied. Although the Galactic model parameters are derived using the exponential functions, Bilir et al. (2006a) showed that the observed vertical distribution in the Galaxy is smoother in the Solar neighbourhood, and is well-approximated by a secans hiperbolicus square function (sech^2). Thus, the number of stars at a distance z from the Galactic plane is described in our study by using both exponential and secans hiperbolicus square functions

$$n(z) = n_0 \exp\left(-\frac{|z|}{H}\right) \quad (3)$$

and

$$n(z) = n_0 \text{sech}^2\left(-\frac{|z|}{H_z}\right), \quad (4)$$

respectively. $n(z)$ based on sech^2 can be also expressed as

$$n(z) = n_0 \left(\frac{4}{\exp(-2z/H_z) + \exp(2z/H_z) + 2} \right) \quad (5)$$

(Bilir et al. 2006a). Here, z is the distance of objects from the Galactic plane and n_0 is the number of stars for $z = 0$ pc. H and H_z are the exponential and sech^2 scale heights, respectively. z is described as $z = z_0 + d \sin(b)$, with b being the Galactic latitude of the star, d distance of the object and z_0 distance of the Sun from the Galactic plane (24 pc; Juric et al. 2008). The relation between the exponential scale height H and the sech^2 scale height H_z is $H = 1.08504 \times H_z$ (Bilir et al. 2006a). To sample the posteriors, we used the Markov Chain Monte Carlo (MCMC) *emcee* package of the affine-invariant ensemble sampler (Goodman & Weare 2010), kindly provided by Foreman-Mackey et al. (2013). To obtain initial model parameters, we used a nonlinear least-squares algorithm (Python library LMFIT). Using these priors, we ran the MCMC to sample the posteriors for 128 initial conditions and tested these walkers in 15,000 steps of chains. Thus, we obtained the most plausible model parameters and their errors through minimising chi-square (χ_{\min}^2).

The best fits to the z -histograms of All CVs and magnetic CVs in the sample are shown in Figure 8. We also demonstrate the 2-D posterior probability distributions of the model parameters sampled by MCMC in Figure 8. The scale height H and the number of stars in the Solar neighbourhood n_0 obtained from the analyses are listed in Table 3.

It is remarkable that exponential and sech^2 functions give very similar scale heights for the two groups in Table 3. Nevertheless, the exponential functions well represent the z -histograms in Figure 8 constructed for All CVs and magnetic CVs in the sample. From Table 3, we found that there is a considerable difference between the scale heights obtained for All CVs and magnetic systems, 375 ± 2 and 281 ± 3 pc, respectively. This can be expected as the median distances of these two groups of systems are 989 and 559 pc, respectively. Thus, we conclude that magnetic CVs are different than All CVs in the sample with respect to the scale height. In addition, as a consequence of reduced

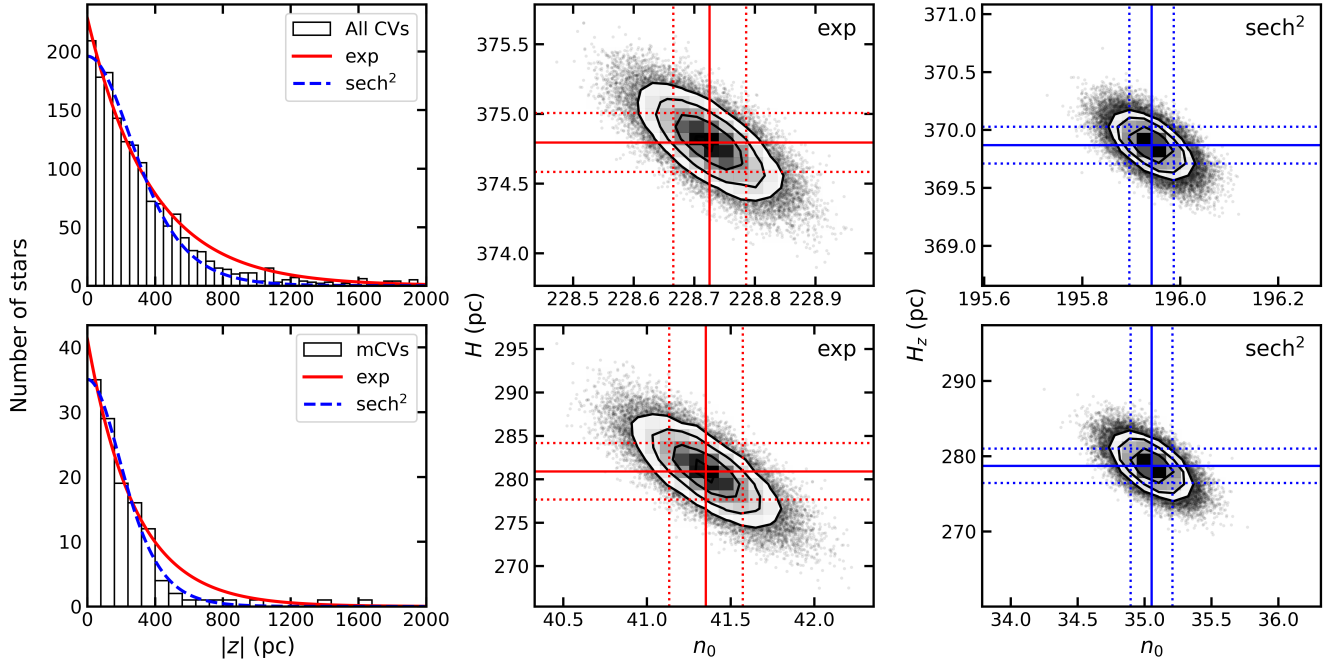


Figure 8. The z -histograms for CVs. The upper panel shows the z -histogram for All CVs in the sample and the lower panel magnetic systems (mCVs). The blue dashed line represents the sech^2 function and the red solid line the exponential function. The 2-D posterior probability distributions of the model parameters sampled by MCMC are demonstrated to the right of the z -histograms.

Table 3. The Galactic model parameters for All CVs and mCVs in the sample. Model functions are given in the third column. Here, exp denotes for exponential function and sech^2 for secans hiperbolicus square function. N is the number of systems in the object group, n_0 is the number of stars in the Solar neighbourhood, H the scale height for the model function.

Group	N	Function	n_0	$H(\text{pc})$
All CVs	1587	exp	229 ± 1	375 ± 2
		sech^2	196 ± 1	370 ± 1
mCVs	124	exp	41 ± 1	281 ± 3
		sech^2	35 ± 1	279 ± 3

magnetic braking with the strong magnetic fields (Li et al. 1994), magnetic CVs evolve slower than non-magnetic systems (Araujo-Betancor et al. 2005). Thus, we expect that their Galactic parameters should be different. Ak et al. (2013) estimated the contribution of thick-disc CVs in the Solar neighbourhood to the Galactic model parameters from the Monte Carlo simulations and found that only about 6 per cent of CVs in the Solar neighbourhood are members of the thick-disc population of the Galaxy. Therefore, the effect of thick disc systems on the scale heights in Table 3 must be negligible.

Another interesting finding is that, if the z histogram of CVs is accepted to be exponential, it must be about 25 missing CVs within the sphere with a radius of about 100 pc with the Sun at the centre, which reminds that the number of period bouncers discovered in sky surveys is less than expected from the population models based on the standard theory. McAllister et al. (2019) found that 30% of donor stars in their sample are likely to be brown dwarfs in period bouncers, while only 5% of CVs are located within 150 pc from the Sun in Pala et al. (2020) included period bouncers.

Although we selected magnetic systems (AM Her or DQ Her type systems) according to their classification in the literature, in fact, it can be unclassified magnetic systems in the sample. In a sense, the sample could be contaminated by them. As a result the scale heights estimated for All CVs in Table 3 could not be reliable. In order to find the effect

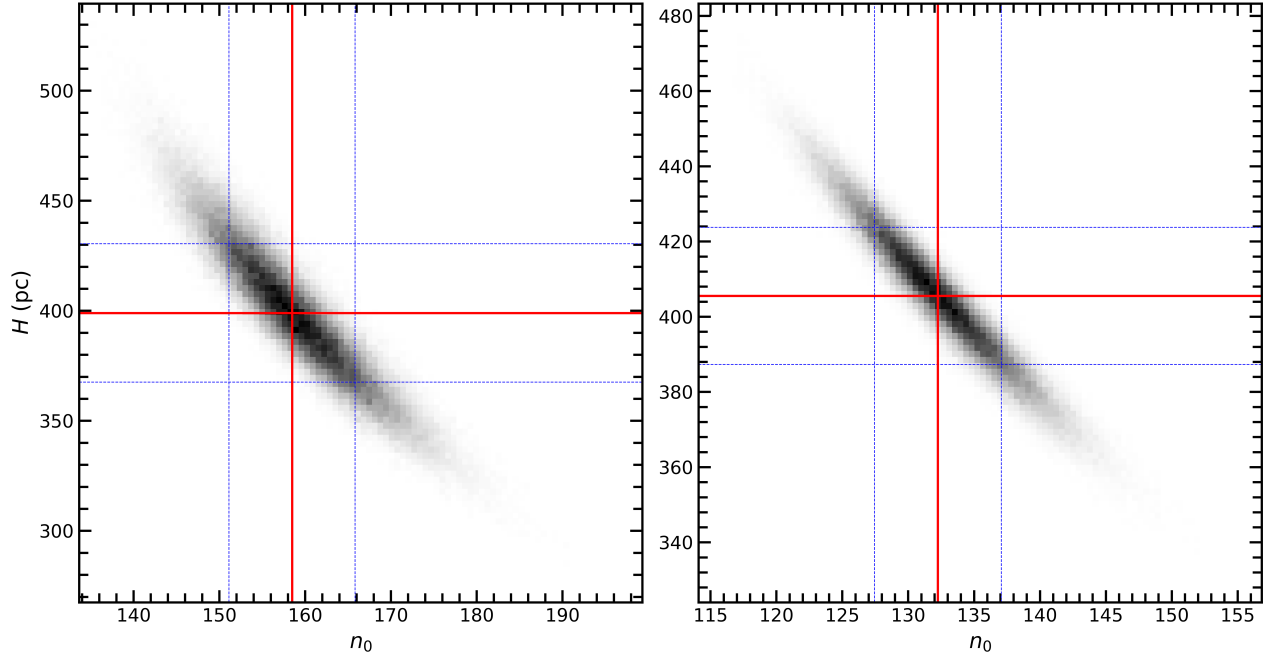


Figure 9. The number of stars for $z = 0$ pc (n_0) versus scale height (H), estimated with 15,000 trials for the Monte Carlo simulations. The simulations were performed for All CVs in the sample, keeping magnetic systems in the sample as they are and assuming 22% of the remaining sample to be magnetic by arbitrary selection. The left and right panels are plotted for exponential and sech^2 scale heights, respectively. Red straight lines show the most probable values. 1σ values are indicated with blue straight lines.

of magnetic system contamination on the scale height of All CVs, we decided to perform Monte Carlo simulations. An inspection shows that about 30% of CVs in the catalogue of Ritter & Kolb (2003) are classified as either AM Her or DQ Her system. Thus, we assumed that 30% of the systems in our sample is magnetic. As we know that 124 of CVs in the sample are classified as magnetic, which is about 8% of objects in this study. Keeping magnetic systems in the sample as they are, 22% of the remaining sample were assumed to be magnetic by arbitrary selection. We calculated n_0 and H for each run of 15,000 trials for the Monte Carlo simulations. Figure 9 shows n_0 versus H for the logarithmic and sech^2 functions. After 15,000 trials for the Monte Carlo simulations performed on All CVs in the sample, the most probable values of the scale heights for the logarithmic and sech^2 functions were found to be 398 ± 31 and 406 ± 18 pc, respectively. Error values are 1σ errors. A comparison with the values in Table 3 shows that these values are in agreement, within errors, with those given for All CVs in the sample and the effect of the magnetic system' contamination on the scale height of all systems can be negligible for our sample. Note that the most probable n_0 values obtained from the Monte Carlo simulations are 158 ± 7 and 132 ± 5 for the logarithmic and sech^2 functions, respectively. Differences of these values from those in Table 3 are expected as the system numbers in different z distances were changed during the simulations.

A comparison of the scale heights found in this study with the ones in Özdönmez et al. (2015) reveals that their results are very different from those listed in Table 3. They found the exponential scale heights to be 213_{-10}^{+11} and 173_{-15}^{+18} pc for All CVs and magnetic systems in their sample, respectively. It is clear that these values are very different than 375 ± 2 and 281 ± 3 pc in Table 3. The scale height of about 375 pc found for All CVs in this study is also considerably larger than those suggested by Patterson (1984, 190 ± 30 pc), van Paradijs, Augusteijn & Stehle (1996, 160-230 pc) and Ak et al. (2008, 158 ± 14 pc). Note that Pala et al. (2020) assumed a scale height of 280 pc for their analysis.

The scale height differences between this study and the previous estimates should be resulted from the number of systems in the analysis and the accuracy of distance estimates. As our data sample is based on reliable distances based on precise trigonometric parallax measurements and it includes the highest number of systems in a similar analysis in the literature, we believe that the results in Table 3 can be confidently used in population studies and further analysis of CVs.

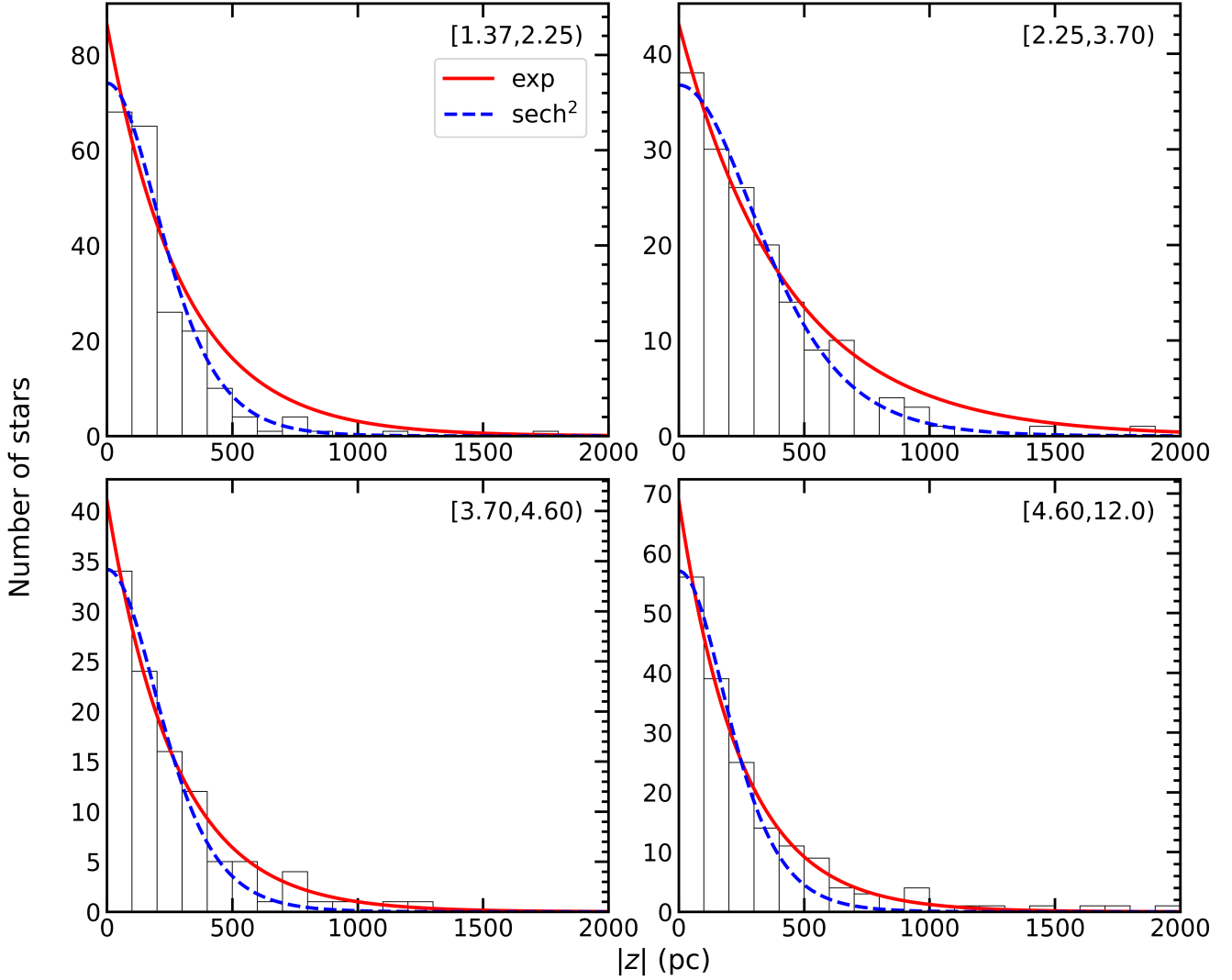


Figure 10. The z -histograms for All CVs in the sample in terms of the orbital period. Orbital period ($P_{\text{orb}}(\text{h})$) intervals are shown in brackets. The best fits to the z -histograms are also presented. The blue dashed line represents the sech^2 function and the red solid line the exponential function.

We also derived the scale height of CVs in terms of the orbital period to find if this Galactic model parameter changes according to the orbital period. In order to compare our results with those in Özdönmez et al. (2015), the CVs in our sample were divided into four-period intervals as defined in their study. Thus, there are 203 systems in the period interval $1.37 \leq P_{\text{orb}}(\text{h}) < 2.25$, 157 systems in $2.25 \leq P_{\text{orb}}(\text{h}) < 3.7$, 105 systems in $3.7 \leq P_{\text{orb}}(\text{h}) < 4.6$ and 171 in $4.6 \leq P_{\text{orb}}(\text{h}) < 12$. The best fits to the z -histograms of CVs grouped according to these period intervals are shown in Figure 10. The scale height H and the number of stars in the Solar neighbourhood n_0 obtained from the minimum χ^2 analysis are listed in Table 4 for the period intervals given above. Since the number of systems is too small for magnetic CVs in these period ranges, we list the Galactic model parameters only for All CVs in the sample.

The z -histograms in Figure 10 are well represented by exponential functions, in general. A comparison of scale heights in Table 4 with those given in Özdönmez et al. (2015) shows the same trend, although the values in this study are more reliable. The scale height increases monotonously from 248 ± 2 to 430 ± 4 pc while the orbital period decreases from 12 to 2.25 h. However, it drops to 300 ± 2 pc for the shortest orbital period CVs with $P_{\text{orb}} < 2.25$ h. We found a similar trend also for the sech^2 function. The scale height for the systems in the interval $2.25 \leq P_{\text{orb}}(\text{h}) < 3.70$ is the highest for all CVs. Note that only $\sim 14\%$ of the systems in this interval are classified as mCV in our sample.

Table 4. The Galactic model parameters for All CVs in the sample in terms of the orbital period $P_{\text{orb}}(\text{h})$. n_0 and H are as defined in Table 3.

$P_{\text{orb}}(\text{h})$	N	Function	n_0	H (pc)
[1.37 , 2.25)	203	exp	86 ± 1	300 ± 2
		sech ²	74 ± 1	286 ± 1
[2.25 , 3.70)	157	exp	43 ± 1	430 ± 4
		sech ²	37 ± 1	424 ± 3
[3.70 , 4.60)	105	exp	41 ± 1	269 ± 4
		sech ²	34 ± 1	278 ± 3
[4.60 , 12.00)	171	exp	69 ± 1	248 ± 2
		sech ²	57 ± 1	258 ± 2

Table 5. The logarithmic and local space densities of CVs. Symbols for subgroups are as in Table 3. N denotes the number of stars in the subgroup, D_0 is the local space density and D^* logarithmic space density.

Group	N	D^*	D_0 ($\times 10^{-6} \text{ pc}^{-3}$)
All CVs	1587	4.83 ± 0.07	$6.8_{-1.1}^{+1.3}$
mCVs	124	4.33 ± 0.09	$2.1_{-0.4}^{+0.5}$

3.3. Space density

Space density is an important parameter for population synthesis studies based on theoretical evolutionary models of a selected object type. The space density of a group of stars is derived by dividing the number of stars in consecutive distances from the Sun to the corresponding partial spherical volumes: $D = N/\Delta V_{i,i+1}$ (Bilir et al. 2006a,b,c). Here, D is the space density, N denotes the number of stars in the partial spherical volume $\Delta V_{i,i+1}$ which is defined by consecutive distances d_i and d_{i+1} from the Sun. The logarithmic space density is preferred to compare the results in the literature, which is defined as $D^* = \log D + 10$. The logarithmic density functions of All CVs and magnetic systems in the Solar neighbourhood are shown in Figure 11, where r^* denotes the centroid distance of the partial spherical volume which is defined as $r^* = [(d_i^3 + d_{i+1}^3)/2]^{1/3}$. The local space density D_0 is the space density estimated for $r^* = 0$ pc from the exponential fits shown in Figure 11. The logarithmic and local space densities of CV groups in the Solar neighbourhood are listed in Table 5.

Table 5 shows that the local space density of All CVs in the sample is $6.8_{-1.1}^{+1.3} \times 10^{-6} \text{ pc}^{-3}$. The space density of magnetic CVs are about three times smaller than that found for all systems, $2.1_{-0.4}^{+0.5} \times 10^{-6} \text{ pc}^{-3}$. The local space density estimation in this study takes into account the CVs located even further than 6 kpc, which corresponds to a large Galactic volume. Note that the median distance of the objects in the sample is 989 pc and the local space density estimation is based on the objects within the completeness limits. Therefore, we believe that the space density values obtained from the CV sample in this study are reliable.

CV population synthesis models based on the standard formation and evolution scenario predicts space densities 10^{-5} - 10^{-4} pc^{-3} (Ritter & Burkert 1986; de Kool 1992; Kolb 1993; Politano 1996; Willems et al. 2005, 2007; Goliaş & Nelson 2015; Belloni et al. 2018) while the space densities found in observational studies are on the order of 10^{-7} - 10^{-4} pc^{-3} (Warner 1974; Patterson 1984, 1998; Thomas & Beuermann 1998; Ringwald 1993; Schwöpe et al. 2002; Araujo-Betancor et al. 2005; Pretorius et al. 2007a,b; Ak et al. 2008; Revnivtsev et al. 2008; Pretorius & Knigge 2012; Pretorius et al. 2013; Schwöpe 2018) In a recent study, Pala et al. (2020) measured the space density of $4.8_{-0.9}^{+0.6} \times 10^{-6}$ and $1.2_{-0.5}^{+0.4} \times 10^{-6} \text{ pc}^{-3}$ for All CVs and mCVs, respectively, from *Gaia* DR2 (Gaia Collaboration 2018). They assumed a scale height of 280 pc for their analysis and their data sample included 42 objects within 150 pc from the Sun. Note that we found a scale height of $H = 375$ pc for All CVs (see Table 3).

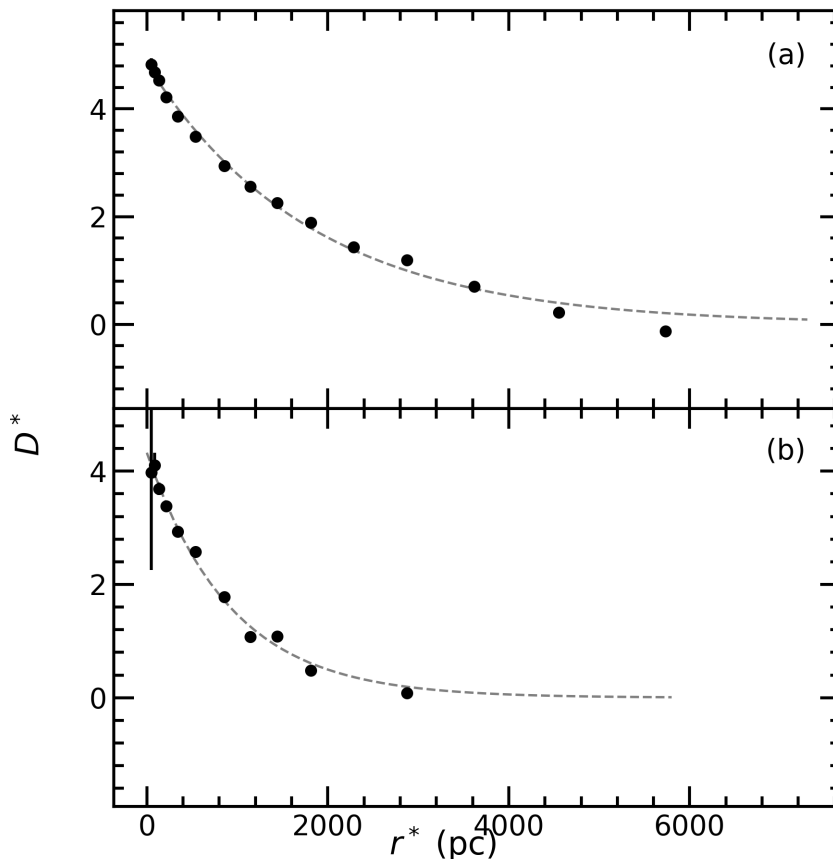


Figure 11. The logarithmic density functions of All CVs (panel a) and mCVs (panel b) in the sample. Dashed lines represent exponential fits applied to the data.

The local space density estimated for All CVs in our sample ($6.8_{-1.1}^{+1.3} \times 10^{-6} \text{ pc}^{-3}$) is 2-20 times smaller than those predicted by population synthesis studies based on the standard evolution scenario. However, it is very similar to the observational space density found by Pala et al. (2020) ($4.8_{-0.9}^{+0.6} \times 10^{-6} \text{ pc}^{-3}$) from *Gaia* DR2 (Gaia Collaboration 2018), within the errors. The local space densities obtained in this study are only about 1.5 times more than those they found. Note that the fraction of mCVs in the whole sample used in this study is about 8%.

3.4. Luminosity function

The luminosity function is defined as the space density of objects in a certain absolute magnitude interval (Karaali et al. 2003, 2004, 2009; Ak et al. 2007). We estimated the logarithmic luminosity functions ϕ for All CVs and magnetic systems and presented them in Table 6, where $\Delta V_{i,i+1}$ is the partial spherical volume which includes the objects located between the distances d_i and d_{i+1} . These distance limits correspond to the bright and faint limiting apparent magnitudes in *G*-band, $9 \leq G \leq 18.5$ mag, for the absolute magnitude M_G interval preferred here. The logarithmic luminosity functions of all systems and magnetic systems are plotted in the lower panel of Figure 12. As can be expected, the luminosity function of All CVs is considerably different than the one estimated for magnetic CVs.

The luminosity function of All CVs in the data sample is plotted in the upper panel of Figure 12, where we also presented the white dwarf luminosity function that demonstrate the collective evolution of white dwarfs (Gaia Collaboration 2021b). As can be seen from Table 6 and Figure 12, besides magnetic systems have a luminosity function smaller than that estimated for All CVs, they span a narrower absolute magnitude interval compared to the absolute magnitude interval of all systems. The comparison of the luminosity functions of white dwarfs and All CVs in our sample reveals that the tendencies of both luminosity functions is almost the same and that the 500 times the luminosity function of All CVs corresponds to the continuation of the luminosity function of white dwarfs towards the brighter absolute magnitudes. A similar comparison was demonstrated by Özdönmez et al. (2015) for CVs in their

Table 6. The logarithmic luminosity functions ϕ of CVs in the sample with $9 \leq G \leq 18.5$ mag. N is the number of stars in the M_G absolute magnitude interval given in the first column. $\Delta V_{i,i+1}$ is the partial spherical volume that includes the objects between the distances d_i and d_{i+1} corresponding to the bright and faint limits in G -band for the absolute magnitude M_G interval. ρ denotes the density and r^* the centroid distance of the partial spherical volume.

M_G (mag)	d_1 (pc)	d_2 (pc)	$\Delta V_{1,2}$ (pc ³)	r^* (kpc)	All CVs			mCVs		
					N	ρ (pc ⁻³)	ϕ	N	ρ (pc ⁻³)	ϕ
[-3,-2)	2512	125893	8.4×10^{15}	99.92	11	1.3×10^{-15}	-14.9	1	1.2×10^{-16}	-15.9
[-2,-1)	1585	79433	2.1×10^{15}	63.05	8	3.8×10^{-15}	-14.4	1	4.8×10^{-16}	-15.3
[-1, 0)	1000	50119	5.3×10^{14}	39.78	25	4.7×10^{-14}	-13.3	1	1.9×10^{-15}	-14.7
[0, 1)	631	31623	1.3×10^{14}	25.10	22	1.7×10^{-13}	-12.8	5	3.8×10^{-14}	-13.4
[1, 2)	398	19953	3.3×10^{13}	15.84	28	8.4×10^{-13}	-12.1	3	9.0×10^{-14}	-13.0
[2, 3)	251	12589	8.4×10^{12}	9.99	87	1.0×10^{-11}	-11.0	5	6.0×10^{-13}	-12.2
[3, 4)	158	7943	2.1×10^{12}	6.30	164	7.8×10^{-11}	-10.1	10	4.8×10^{-12}	-11.3
[4, 5)	100	5012	5.3×10^{11}	3.98	229	4.3×10^{-10}	-9.4	14	2.7×10^{-11}	-10.6
[5, 6)	63	3162	1.3×10^{11}	2.51	275	2.1×10^{-09}	-8.7	12	9.1×10^{-11}	-10.0
[6, 7)	40	1995	3.3×10^{10}	1.58	210	6.3×10^{-09}	-8.2	8	2.4×10^{-10}	-9.6
[7, 8)	25	1259	8.4×10^9	1.00	159	1.9×10^{-08}	-7.7	13	1.6×10^{-09}	-8.8
[8, 9)	16	794	2.1×10^9	0.63	159	7.6×10^{-08}	-7.1	24	1.1×10^{-08}	-7.9
[9,10)	10	501	5.3×10^8	0.40	99	1.9×10^{-07}	-6.7	10	1.9×10^{-08}	-7.7
[10,11)	6	316	1.3×10^8	0.25	65	4.9×10^{-07}	-6.3	10	7.6×10^{-08}	-7.1
[11,12)	4	200	3.4×10^7	0.16	28	8.4×10^{-07}	-6.1	6	1.8×10^{-07}	-6.7
[12,13)	3	126	8.4×10^6	0.10	7	8.4×10^{-07}	-6.1	1	1.2×10^{-07}	-6.9

data sample and white dwarfs in the Anglo Australian Telescope survey (Boyle 1989) and the Palomar Green survey (Fleming, Liebert & Green 1986).

The single white dwarf masses are significantly smaller than those of the white dwarfs in CVs (see Zorotovic & Schreiber 2020, and references therein) and it is claimed that the white dwarf mass does not depend on the orbital period (McAllister et al. 2019; Pala et al. 2022). In addition, the mass of CV white dwarfs does not show a monotonous increase during the evolution of the system and the contribution of the primary component to the total radiation of a CV is dominant -or much higher- in UV rather than that in optical (Gänsicke 2000). Simulations performed by Hillman et al. (2020) predicts that the white dwarf masses in CVs decrease monotonically, by only a few per cent throughout the evolution of cataclysmic variable. Therefore, it is unlikely that the trend of CV luminosity function in the upper panel of Figure 12 reflects the evolution of the white dwarf companion of these systems. In any case, this comparison shows that we find one CV for about 500 white dwarfs in the Solar neighbourhood.

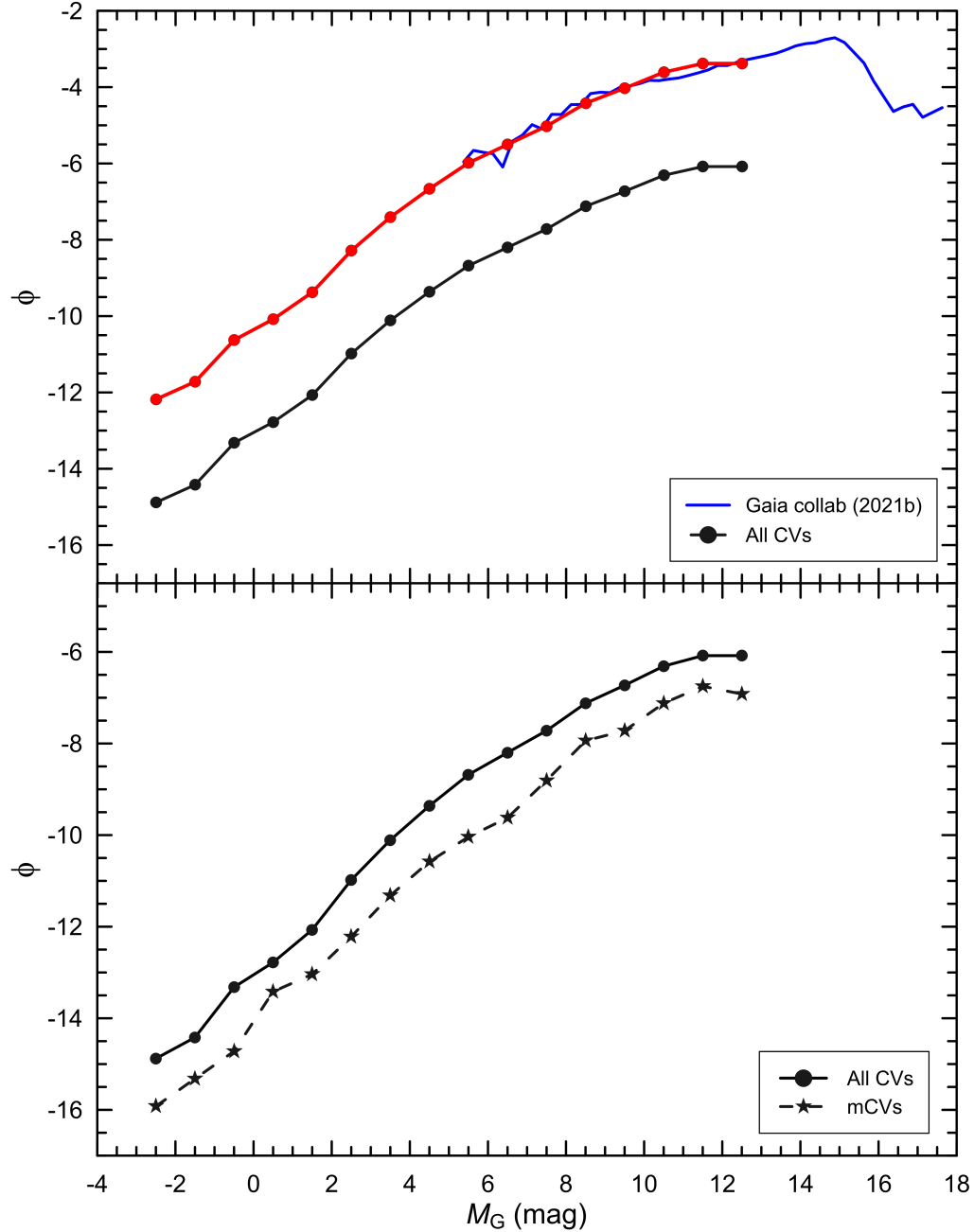


Figure 12. Logarithmic luminosity functions of CVs. Lower panel shows luminosity functions for All CVs and mCVs. Upper panel demonstrates the logarithmic luminosity function for All CVs in the sample. Red line represent the 500 times the luminosity function of All CVs and the blue line logarithmic luminosity function of white dwarfs taken from [Gaia Collaboration \(2021b\)](#).

4. CONCLUSIONS

The spatial distribution, Galactic model parameters and luminosity function of cataclysmic variables were precisely derived using distances from [Bailer-Jones et al. \(2021\)](#), who re-estimated trigonometric parallaxes of ESA’s *Gaia* DR3 ([Gaia Collaboration 2021a](#)). We compared distances obtained from [Bailer-Jones et al. \(2021\)](#) and *Gaia* DR3 data ([Gaia Collaboration 2022](#)) found that the scatter is too much for the systems $G \geq 18.5$ mag. Thus, the data sample in this study includes CVs with $9 \leq G \leq 18.5$ mag. Number of CVs in the sample decreased from 10,852 to 1,587, with 124 of them are magnetic systems, by preventing the misidentification of CVs due to adjacent objects, checking

for duplication and by also taking into account the quality flags of parallax measurements and completeness limits of the data.

Projected positions of CVs on the Galactic plane ($X - Y$ plane) and on a plane perpendicular to it ($X - Z$ plane) demonstrate that systems in the sample are symmetrically distributed about the Galactic plane, in general. So, we conclude that there is no considerable bias according to the spatial distribution of CVs in our study. The median distances of objects in the sample are 989 and 559 for All CVs and magnetic systems, respectively.

The exponential scale heights were found to be 375 ± 2 and 281 ± 3 for All CVs and mCVs in the sample, respectively. Thus, we conclude that a scale height of 375 pc can be used in CV studies, in general. This value is considerably larger than those previously suggested in observational studies (Patterson 1984; van Paradijs et al. 1996; Ak et al. 2008). It is also significantly larger than that estimated by Özdönmez et al. (2015). Monte Carlo simulations showed that the magnetic system' effect on the scale height of all systems can be negligible for the sample.

It seems that it must be 25 missing CVs within the sphere with a radius of about 100 pc with the Sun at the centre. This reminds that the number of period bouncers discovered in sky surveys is less than expected from the population models based on the standard theory. Note that McAllister et al. (2019) found that 30% of donor stars in their sample are likely to be brown dwarfs in period bouncers.

The exponential scale heights of All CVs derived in terms of the orbital period shows that the scale height increases from 248 ± 2 to 430 ± 4 pc with the orbital period decreases from 12 to 2.25 h, and it almost suddenly drops to 300 ± 2 pc for the shortest orbital period CVs with $P_{\text{orb}} < 2.25$ h. A similar trend was also found in Özdönmez et al. (2015). Note that Pretorius et al. (2007b) modelled the Galactic population of CVs adopting 120, 260 and 450 pc for long, normal short orbital period systems and period bouncers, respectively.

The local space density of All CVs and magnetic systems in the sample was estimated to be $6.8^{+1.3}_{-1.1} \times 10^{-6}$ and $2.1^{+0.5}_{-0.4} \times 10^{-6}$ pc $^{-3}$, respectively. The space densities estimated here for All CVs and magnetic systems are in agreement with those calculated by Pala et al. (2020), who used 42 CVs within 150 pc from the Sun with data obtained from *Gaia* DR2 (Gaia Collaboration 2018), within errors. They measured the space densities of $4.8^{+0.6}_{-0.9} \times 10^{-6}$ and $1.2^{+0.4}_{-0.5} \times 10^{-6}$ pc $^{-3}$ for all CVs and magnetic CVs, respectively. We claim that the space density values in our study are the most reliable estimates ever found. The measurements in this study strengthen the discrepancy between CV space densities obtained from observations and those predicted by population synthesis models based on the standard formation and evolution theory of these systems. If the population synthesis models are correct, this disagreement between the theory and observations means that the current CV surveys are incomplete as they missed almost all very low \dot{M} systems and CVs in the period gap, through which the life time of a CV is predicted to be longer (Hillman et al. 2020), and period bouncers.

The logarithmic luminosity functions derived for CVs in the sample are in agreement with those shown in Özdönmez et al. (2015). The trend of the logarithmic luminosity functions of CVs and white dwarfs are very similar. Although 500 times the luminosity function of CVs looks like the extension of the white dwarf luminosity function towards the brighter absolute magnitudes, it is not likely that this similarity indicates the evolution of white dwarf companion of CVs as the mass of CV white dwarfs does not show a monotonous increase during the evolution of the system and contribution of the primary component to the total radiation of a CV is dominant in UV (Gänsicke 2000; Pala et al. 2022).

To conclude, the results in this study can be used in population studies and analysis of cataclysmic variables. We believe that the further *Gaia* observations of cataclysmic variables and surveys focused on low \dot{M} CVs and fainter systems will lead to not only larger datasets but also more precise distance measurements for these systems. Such observational results will allow us to obtain more detailed and confident observational Galactic model parameters to test population synthesis models.

5. ACKNOWLEDGMENTS

We would like to thank Michael Shara, the referee, for his useful and constructive comments concerning the manuscript. This work has been supported in part by the Scientific and Technological Research Council of Turkey (TÜBİTAK) 119F072. This work has been supported in part by Istanbul University: Project number NAP-33768. This study is a part of the PhD thesis of Remziye Canbay. This work has made use of data from the European Space Agency (ESA) mission *Gaia* (<https://www.cosmos.esa.int/gaia>), processed by the *Gaia* Data Processing and Analysis Consortium (DPAC, <https://www.cosmos.esa.int/web/gaia/dpac/consortium>). Funding for DPAC has been provided by national institutions, in particular, the institutions participating in the *Gaia* Multilateral Agreement. This research

has made use of NASA's (National Aeronautics and Space Administration) Astrophysics Data System Bibliographic Services and the SIMBAD Astronomical Database, operated at CDS, Strasbourg, France and NASA/IPAC Infrared Science Archive and Extragalactic Database (NED), which is operated by the Jet Propulsion Laboratory, California Institute of Technology, under contract with the National Aeronautics and Space Administration.

REFERENCES

- Abril, J., Schmidtobreick, L., Ederoclite, A., López-Sanjuan, C., 2020, *MNRAS*, 492, L40
- Ak, S., Bilir, S., Karaali, S., Buser, R., 2007, *AN*, 328, 169
- Ak, T., Bilir, S., Ak, S., Eker, Z., 2008, *NewA*, 13, 133
- Ak, T., Bilir, S., Ak, S., et al., 2010, *NewA*, 15, 491
- Ak, T., Bilir, S., Güver, T., et al., 2013, *NewA*, 22, 7
- Ak, T., Bilir, S., Özdönmez, A., et al., 2015, *Ap&SS*, 357, 72
- Alfonso-Garzón, J., Domingo, A., Mas-Hesse, J. M., Giménez, A., 2012, *A&A*, 548, A79
- Altan, M., Kato, T., Ishioka, R., et al., 2019, *MNRAS*, 489, 1451
- Araujo-Betancor, S., Gänsicke, B.T., Long, K.S., et al., 2005, *ApJ*, 622, 589
- Avilés, A., Arias, I., Chávez, C. E., et al., 2020, *RMxAA*, 56, 11
- Bahcall, J.N., Soneira, R.M., 1980, *ApJS* 44, 73
- Bailer-Jones, C.A.L., Rybizki, J., Fouesneau, M., et al., 2018, *AJ*, 156, 11
- Bailer-Jones, C.A.L., Rybizki, J., Fouesneau, M., et al., 2021, *AJ*, 161, 147
- Belloni, D., Schreiber, M. R., Zorotovic, M., et al., 2018, *MNRAS*, 478, 5626
- Belloni, D., Schreiber, M.R., Pala, A.F., et al., 2020, *MNRAS*, 491, 5717
- Belloni, D., Schreiber, M.R., 2020, *MNRAS*, 492, 1523
- Bernardini, F., de Martino, D., Mukai, K., et al., 2019, *MNRAS*, 489, 1044
- Beuermann, K., Burwitz, V., Reinsch, K., et al., 2021, *A&A*, 645, A56
- Bilir, S., Karaali, S., Ak, S., et al., 2006a, *NewA* 12, 234
- Bilir, S., Karaali, S., Güver, T., et al., 2006b, *AN*, 327, 72
- Bilir, S., Karaali, S., Gilmore, G., 2006c, *MNRAS* 366, 1295
- Bilir, S., Cabrera-Lavers, A., Karaali, S., et al., 2008, *PASA*, 25, 69
- Bond, H. E., Miszalski, B., 2018, *PASP*, 130, 094201
- Bovy, J., Rix, H.-W., Green, G.M., et al., 2016, *ApJ*, 818, 130
- Boyle, B.J., 1989, *MNRAS*, 240, 549
- Breus, V., Petrík, K., Zola, S., 2019, *MNRAS*, 488, 4526
- Bruch, A., Diaz, M. P., 2017, *NewA*, 50, 109
- Bruch, A., 2019, *MNRAS*, 489, 2961
- Cabrera-Lavers, A., Bilir, S., Ak, S., et al., 2007, *A&A*, 464, 565
- Cardelli, J. A., Clayton, G. C., Mathis, J. S., 1989, *ApJ*, 345, 245
- Chen, X., Wang, S., Deng, L., et al., 2020, *ApJS*, 249, 18
- Copperwheat, C. M., Marsh, T. R., Dhillon, V. S., et al., 2011, *MNRAS*, 413, 3068
- Coppejans, D. L., Körding, E. G., Knigge, C., et al., 2016, *MNRAS*, 456, 4441
- Dai, Z., Szkody, P., Thorstensen, J. R., Medagangoda, N. I., 2020, *ApJ*, 893, 58
- de Kool, M., 1992, *A&A*, 261, 188
- Downes, R.A., Webbink, R.F., Shara, M.M., et al., 2001, *PASP*, 113, 764
- Drake, A. J., Graham, M. J., Djorgovski, S. G., et al., 2014, *ApJS*, 213, 9
- Duerbeck, H.W., 1984, *Ap&SS*, 99, 363
- Fleming, T.A., Liebert, J., Green, R.F., 1986, *ApJ*, 308, 176
- Foreman-Mackey, D. Hogg, D. W., Lang, D., Goodman, J., 2013, *PASP*, 125, 306
- Gabdeev, M. M., Shimansky, V. V., Borisov, N. V., et al., 2019, *AstBu*, 74, 308
- Gaia Collaboration, Prusti, T., de Bruijne, J. H. J., et al., 2016, *A&A*, 595, A1
- Gaia Collaboration, Brown, A.G.A., Vallenari, A., Prusti, T., et al., 2018, *A&A*, 616, 1
- Gaia Collaboration, Brown, A.G.A., Vallenari, A., Prusti, T., et al., 2021a, *A&A*, 649, 1
- Gaia Collaboration, Smart, R.L., Sarro, L.M., Rybizki, J., et al., 2021b, *A&A*, 649, 6
- Gaia Collaboration, 2022, *A&A*, arXiv:2208.00211
- Gänsicke, B.T., 2000, *RvMA*, 13, 151
- Gänsicke, B.T., Dillon, M., Southworth, J., et al., 2009, *MNRAS*, 397, 2170
- Gasque, L. C., Hening, C. A., Hviding, R. E., et al., 2019, *AJ*, 158, 156
- Goliash, J., Nelson, L., 2015, *ApJ*, 809, 80
- González-Buitrago, D., Tovmassian, G., Zharikov, S., et al., 2013, *A&A*, 553, A28.
- Goodman, J., Weare, J., 2010, *CAMCS*, 5, 65
- Hambusch, F.-J., 2014, *JAVSO*, 42, 324
- Hamilton-Drager, C. M., Lane, R. I., Recine, K. A., et al., 2018, *AJ*, 155, 58

- Han, Z.-T., Qian, S.-B., Voloshina, I., et al., 2016, *RAA*, 16, 156
- Halpern, J. P., Thorstensen, J. R., 2015, *AJ*, 150, 170
- Halpern, J.P., Thorstensen, J.R., Cho, P., et al., 2018, *AJ*, 155, 247
- Hardy, L. K., McAllister, M. J., Dhillon, V. S., et al., 2017, *MNRAS*, 465, 4968
- Hellier, C., 2001, *Cataclysmic Variable Stars, How and why they vary*. Springer-Praxis Books in Astronomy and Space Sciences, Cornwall, UK. (ISBN 978-1-85233-211-2)
- Hernández Santisteban, J.V., Knigge, C., Pretorius, M. L., et al., 2018, *MNRAS*, 473, 3241
- Hillman, Y., Shara, M.M., Prialnik, D., Kovetz, A., 2020, *Nature Astronomy*, 4, 886
- Hofmann, F., Ponti, G., Haberl, F., Clavel, M., 2018, *A&A*, 615, L7
- Howell, S.B., Nelson, L.A., Rappaport, S., 2001, *ApJ*, 550, 897
- Hurley, J.R., Tout, C.A., Pols, O.R., 2002, *MNRAS*, 329, 897
- Hümmerich, S., Bernhard, K., Srdoc, G., 2014, *OEJV*, 167, 1
- Joshi, A., Pandey, J. C., Raj, A., et al., 2020, *MNRAS*, 491, 201
- Jurić, M., Ivezić, Z., Brooks, A., et al., 2008, *ApJ* 673, 864
- Kalomeni, B., Nelson, L., Rappaport, S., et al., 2016, *ApJ*, 833, 83
- Karaali, S., Ak, S. G., Bilir, S., et al., 2003, *MNRAS*, 343, 1013
- Karaali, S., Bilir, S., Hamzaoglu, E., 2004, *MNRAS*, 355, 307
- Karaali, S., Bilir, S., Yaz, E., et al., 2007, *PASA*, 24, 208
- Karaali, S., Hamzaoglu, E., Bilir, S., 2009, *Ap&SS*, 324, 23
- Kato, T., Imada, A., Uemura, M., et al., 2009, *PASJ*, 61, S395
- Kato, T., Hamsch, F.-J., Maehara, H., et al., 2013, *PASJ*, 65, 23
- Kato, T., Hamsch, F.-J., Dubovsky, P.A., et al., 2015, *PASJ*, 67, 105
- Kato, T., Hamsch, F.-J., Monard, B., et al. 2016, *PASJ*, 68, 65
- Kato, T., Isogai, K., Hamsch, F.-J., et al., 2017, *PASJ*, 69, 75
- Kato, T., 2019, *PASJ*, 71, 20
- Kato, T., Isogai, K., Wakamatsu, Y., et al., 2020, *PASJ*, 72, 14
- Kato, T., 2020, *PASJ*, 72, L2
- King, A.R., 1988, *QJRAS*, 29, 1
- Knigge, C., 2011, *Evolution of compact binaries*. ASP Conference Proceedings, 447, Linda Schmidtobreick, Matthias R. Schreiber, and Claus Tappert (eds.), 3
- Knigge, C., Baraffe, I., Patterson, J., 2011, *ApJS*, 194, 28
- Koen, C., O'Donoghue, D., 1995, *ApJS*, 101, 347
- Kolb, U., 1993, *A&A*, 271, 149
- Kozhevnikov, V. P., 2003, *A&A*, 398, 267
- Kozhevnikov, V. P., 2014, *Ap&SS*, 349, 361
- Kozhevnikov, V. P., 2017, *Ap&SS*, 362, 144
- Kozhevnikov, V. P., 2018, *Ap&SS*, 363, 130
- Kozhevnikov, V. P., 2019, *Ap&SS*, 364, 208
- Li, J.K., Wu, K.W., Wickramasinghe, D.T., 1994, *MNRAS*, 268, 61L
- Littlefair, S.P., Dhillon, V.S., Marsh, T. R., et al., 2008, *MNRAS*, 388, 1582
- Liu, W.-M., Li, X.-D., 2019, *ApJ*, 870, 22
- Marshall, D.J., Robin, A.C., Reylé, C., et al., 2006, *A&A*, 453, 635
- Masci, F. J., Laher, R. R., Rusholme, B., et al., 2019, *PASP*, 131, 018003
- Mason, E., Orio, M., Mukai, K., et al., 2013, *MNRAS*, 436, 212
- McAllister, M. J., Littlefair, S. P., Baraffe, I., et al., 2015, *MNRAS*, 451, 114
- McAllister, M.J., Littlefair, S.P., Dhillon, V.S., et al., 2017, *MNRAS*, 467, 1024
- McAllister, M., Littlefair, S.P., Parsons, S.G., et al., 2019, *MNRAS*, 486, 5535
- Metzger, B.D., Zenati, Y., Chomiuk, L., J.S. Ken, Strader, J., 2021, *ApJ*, 923, 100
- Mukai, K., Zietsman, E., Still, M., 2009, *ApJ*, 707, 652
- Myers, G., Patterson, J., de Miguel, E., et al., 2017, *PASP*, 129, 044204
- Nesci, R., Tuvikene, T., Gualandi, R., 2019, *OEJV*, 196, 1
- Neustroev, V.V., Marsh, T.R., Zharikov, S.V., et al., 2017, *MNRAS*, 467, 597
- Özdönmez, A., Ak, T., Bilir, S., 2015, *NewA*, 34, 234
- Pal, P. S., Tam, P. H. T., Liang, W., et al., 2020, *ApJL*, 895, L36
- Pala, A.F., Gänsicke, B.T., Townsley, D., et al., 2017, *MNRAS*, 466, 2855 .
- Pala, A. F., Schmidtobreick, L., Tappert, C., et al., 2018, *MNRAS*, 481, 2523
- Pala, A.F., Gänsicke, B.T., Breedt, E., et al., 2020, *MNRAS*, 494, 3799
- Pala, A.F., Gänsicke, B.T., Belloni, D., et al., 2022, *MNRAS*, 510, 6110
- Paterson, K., Woudt, P. A., Warner, B., et al., 2019, *MNRAS*, 486, 2422
- Patterson, J., 1984, *ApJS*, 54, 443

- Patterson, J., 1998, *PASP*, 110, 1132
- Patterson J., Thorstensen J. R., Kemp J., et al., 2003, *PASP*, 115, 1308
- Patterson, J., Kemp, J., Harvey, D.A., et al., 2005, *PASP*, 117, 1204
- Patterson, J., 2011, *MNRAS*, 411, 2695
- Plavchan, P., Jura, M., Kirkpatrick, J. D., et al., 2008, *ApJS*, 175, 191
- Politano, M., 1996, *ApJ*, 465, 338
- Pretorius, M.L., Knigge, C., O'Donoghue, D., et al., 2007a, *MNRAS*, 382, 1279
- Pretorius, M.L., Knigge, C., Kolb, U., 2007b, *MNRAS*, 374, 1495
- Pretorius, M.L., Knigge, C., 2012, *MNRAS*, 419, 1442
- Pretorius, M.L., Knigge, C., Schwöpe, A.D., 2013, *MNRAS*, 432, 570
- Revnivtsev, M., Lutovinov, A., Churazov, E., et al., 2008, *A&A*, 491, 209
- Ringwald, F.A., 1993, *PASP*, 105, 805
- Ringwald, F. A., Velasco, K., 2012, *NewA*, 17, 108
- Ritter, H., Burkert, A., 1986, *A&A*, 158, 161
- Ritter, H., Kolb, U., 2003, *A&A*, 404, 301
- Rodríguez-Gil, P., Torres, M. A. P., 2005, *A&A*, 431, 289
- Rodríguez-Gil, P., Schmidtbreick, L., Long, K. S., et al., 2012, *MNRAS*, 422, 2332
- Rude, G. D., Ringwald, F. A., 2012, *NewA*, 17, 442
- Rude, G. D., Ringwald, F. A., 2012, *NewA*, 17, 453
- Ruiz-Carmona, R., Groot, P. J., Steeghs, D., 2020, *MNRAS*, 491, 2217
- Rutkowski, A., Pietrukowicz, P., Olech, A., et al., 2011, *AcA*, 61, 345
- Samus', N. N., Kazarovets, E. V., Durlevich, O. V., et al., 2017, *ARep*, 61, 80
- Sarkar, A., Tout, C.A., 2022, *MNRAS*, 513, 4169
- Schaefer, B. E., 2021, *RNAAS*, 5, 150
- Schlafly, E.F., Finkbeiner, D.P., 2011, *ApJ*, 737, 103
- Schlegel, D.J., Finkbeiner, D.P., Davis, M., 1998, *ApJ*, 500, 525
- Schwöpe, A.D., Brunner, H., Buckley, D., et al., 2002, *A&A*, 396, 895
- Schwöpe, A.D., 2018, *A&A*, 619, 62
- Schwöpe, A.D., Worpel, H., Webb, N.A., et al., 2020, *A&A*, 637, 35
- Schreiber, M.R., Zorotovic, M., Wijnen, T.P.G., 2016, *MNRAS*, 455, L16
- Shafter, A. W., Misselt, K. A., 2006, *ApJ*, 644, 1104
- Sheets, H. A., Thorstensen, J. R., Peters, C. J., et al., 2007, *PASP*, 119, 494
- Steiner, J. E., Oliveira, A. S., Torres, C. A. O., Daminieli, A., 2007, *A&A*, 471, L25
- Sterken, C., Vogt, N., Schreiber, M. R., Uemura, M., Tuvikene, T., 2007, *A&A*, 463, 1053
- Szkody, P., Anderson, S.F., Agüeros, M., et al., 2002, *AJ*, 123, 430
- Szkody, P., Fraser, O., Silvestri, N., et al., 2003, *AJ*, 126, 1499
- Szkody, P., Henden, A., Fraser, O., et al., 2004, *AJ*, 128, 1882
- Szkody, P., Henden, A., Fraser, O., et al., 2005, *AJ*, 129, 2386
- Szkody, P., Henden, A., Agüeros, M., et al., 2006, *AJ*, 131, 973
- Szkody, P., Henden, A., Mannikko, L., et al., 2007, *AJ*, 134, 185
- Szkody, P., Anderson, S.F., Brooks, K., et al., 2011, *AJ*, 142, 181
- Szkody P., Albright M., Linnell A. P., et al., 2013, *PASP*, 125, 1421
- Szkody, P., Everett, M.E., Dai, Z., Serna-Grey, D., 2018, *AJ*, 155, 28
- Tappert, C., Schmidtbreick, L., Vogt, N., Ederoclite, A., 2013, *MNRAS*, 436, 2412
- Thomas, H.-C., Beuermann, K., 1998, in Breitschwerdt D., Freyberg M. J., Truemper J., eds, *Lecture Notes in Physics*, Berlin Springer Verlag Vol. 506, IAU Colloq. 166: The Local Bubble and Beyond. pp 247–250
- Thorstensen, J. R., Fenton, W. H., 2003, *PASP*, 115, 37
- Thorstensen, J. R., Peters, C. S., Skinner, J. N., 2010, *PASP*, 122, 1285
- Thorstensen, J. R., Skinner, J. N., 2012, *AJ*, 144, 81
- Thorstensen, J. R., Alper, E. H., Weil, K. E., 2016, *AJ*, 152, 226
- Thorstensen, J. R., Ringwald, F. A., Taylor, C. J., et al., 2017, *RNAAS*, 1, 29
- Thorstensen, J. R., 2020, *AJ*, 160, 6
- Thorstensen, J. R., Motsoaledi, M., Woudt, P. A., et al., 2020, *AJ*, 160, 70
- Uemura, M., Kato, T., Nogami, D., Ohsugi, T., 2010, *PASJ*, 62, 613
- Unda-Sanzana, E., Marsh, T.R., Gänsicke, B.T., et al., 2008, *MNRAS*, 388, 889
- van Paradijs, J., Augusteijn, T., Stehle, R., 1996, *A&A*, 31, 93
- Vogt, N., Tappert, C., Puebla, E. C., et al., 2018, *MNRAS*, 478, 5427
- Warner, B., 1974, *MNSSA*, 33, 21
- Warner, B., 1995, *Cataclysmic Variable Stars*. Cambridge University Press, Cambridge. (Online ISBN 9780511586491)
- Watson, C. L., Henden, A. A., Price, A., 2006, *SASS*, 25, 47

- Weil, K. E., Thorstensen, J. R., Haberl, F., 2018, *AJ*, 156, 231
- Willems, B., Kolb, U., Sandquist, E.L., Taam, R.E., Dubus, G., 2005, *ApJ*, 635, 1263
- Willems, B., Kolb, U., Sandquist, E.L., Taam, R.E., Dubus, G., 2007, *ApJ*, 657, 465
- Wils, P., Krajci, T., Hamsch, F.-J., Muylaert, E., 2011, *IBVS*, 5982, 1
- Worpel, H., Schwobe, A. D., Traulsen, I., Mukai, K., Ok, S., 2018, *A&A*, 617, A52
- Yu, Z., Thorstensen, J.R., Rappaport, S., et al., 2019, *MNRAS*, 489, 1023
- Zorotovic, M., Schreiber, M.R., 2017, *MNRAS*, 466, L63
- Zorotovic, M., Schreiber, M.R., 2020, *Advances in Space Research*, 66, 1080
- Zubareva, A. M., Pavlenko, E. P., Andreev, M. V., et al., 2011, *ARep*, 55, 224